JOURNAL OF GEOPHYSICAL RESEARCH, VOL. 112, D12302, doi:10.1029/2006JD007992, 2007

Global source attribution of tropospheric ozone: Long-range transport from various source regions

K. Sudo[1,2] and H. Akimoto[2]

Received 3 September 2006; revised 1 March 2007; accepted 15 March 2007; published 16 June 2007.

[1] We examine contributions from various source regions to global distributions and budgets of tropospheric ozone (O_3) in the context of intercontinental transport, using tagged tracer simulation with a global chemical transport model. For tagging O_3, we consider regional separation of the model domain on the basis of the distributions of O_3 chemical production. We define 14 polluted source regions (14 tracers) in the boundary layer (North America, Europe, China, etc.) and 8 regions (8 tracers) in the free troposphere; O_3 production in the remaining (remote) tropospheric region and O_3 transport from the stratosphere are also tagged as separate tracers. O_3 transport from the polluted source regions like North America, Europe, and Asia generally accounts for more than 40% of ozone abundances even in remote locations. O_3 exports from boundary layer in China and Asian free troposphere are discerned through much of the Northern Hemisphere, suggesting significant and extensive impacts of eastern Asian pollution. In particular, O_3 from Asian free troposphere plays the most important roles in distribution and seasonal variation of O_3 in the middle-upper troposphere almost globally. In June–September, the model calculates a large O_3 contribution (5–10 ppbv) from Asian free troposphere in the upper troposphere over the South Pacific associated with long-range interhemispheric transport from Asia to the southern midlatitudes (via the western Indian Ocean, Africa, and Atlantic) in the upper troposphere. O_3 transported from biomass burning regions such as South America, Africa, and Australia widely distributes in the Southern Hemisphere. Our simulation demonstrates that there is a significant interhemispheric O_3 transport from South America to the northern midlatitudes in the upper troposphere which reaches Japan, North Pacific, and the United States in conjunction with O_3 export from North Africa. Our tagged O_3 simulation estimates that the annual mean global tropospheric O_3 burden, as calculated to be 344 Tg in this study, comes from chemical production in the source regions (48%) and in the remote regions (29%) and from stratosphere-troposphere exchange (23%).

Citation: Sudo, K., and H. Akimoto (2007), Global source attribution of tropospheric ozone: Long-range transport from various source regions, *J. Geophys. Res.*, *112*, D12302, doi:10.1029/2006JD007992.

1. Introduction

[2] Tropospheric ozone (O_3) is recognized as one of the key factors to control global-scale changes in climate [*Gauss et al.*, 2003, 2006] and air quality [*Akimoto*, 2003]. The effect of tropospheric ozone increase on climate since preindustrial times has typically been estimated to be a global mean radiative forcing between 0.3 and 0.5 W m^{-2} [*Forster et al.*, 1996; *Mickley et al.*, 1999; *Gauss et al.*, 2006]. Unlike well-mixed greenhouse gases, tropospheric ozone and its radiative forcing exhibits spatially and temporally inhomogeneous distributions, being generally larger in the polluted source regions, as a result of its short chemical lifetime (a week to a month). This inhomogeneous distribution of radiative forcing from tropospheric ozone increase can cause climate change with a large regional variability [*Mickley et al.*, 2004]. Tropospheric ozone distribution is basically determined by the combination of transport and photochemical formation processes under the existence of natural and anthropogenic sources like precursors emitted over the industrialized regions as studied by previous studies [e.g., *Li et al.*, 2001]. Transport process also plays a key role in intercontinental and hemispheric pollution issues [e.g., *Jacob et al.*, 1999; *Wild et al.*, 2004]. For better understanding and projection of global ozone changes as associated with the rising Asian continental outflow of pollutants and their impacts on climate and air quality, it is required to clarify the detailed origins of tropospheric ozone at the global scale focusing on the transport and chemical processes.

[3] In a very classic concept, the stratosphere was considered to be the main source of tropospheric ozone [*Junge*,

[1]Graduate School of Environmental Studies, Nagoya University, Nagoya, Japan.
[2]Frontier Research Center for Global Change, JAMSTEC, Yokohama, Japan.

0148-0227/07/2006JD007992$09.00

1962]. Recent studies, however, demonstrate that most of the tropospheric ozone abundance is attributed to photochemical ozone production driven by the smog reaction within the troposphere as associated with air pollution rather than to the transport from the stratosphere [*Roelofs and Lelieveld*, 1997; *Li et al.*, 2002a; *von Kuhlmann et al.*, 2003]. More recently, there are an increasing number of studies which attempt to assess impacts of pollution in the industrialized regions such as the United States, Europe, and Asia on the regional and hemispheric levels of oxidants including ozone [*Holloway et al.*, 2003].

[4] These studies generally pay a particular attention to the major long-range transport pathways in the Northern Hemisphere (NH) such as the typical transport pathway from Asia to North America across the Pacific (the trans-Pacific). *Stohl et al.* [2002] examined pathways and timescales for intercontinental transport of passive CO tracers using a Lagrangian model.

[5] *Berntsen et al.* [1999] and *Jacob et al.* [1999, 2003] studied transport of ozone and related species over the trans-Pacific pathway and evaluated influences of Asian emissions on air quality in the United States. *Li et al.* [2002a] and *Auvray and Bey* [2005] similarly investigated impacts of long-range transport from Asia and North America on surface ozone levels in Europe. In addition, *Wild et al.* [2004] examined the characteristics of the trans-Eurasian transport and assessed impacts of European and North American anthropogenic emissions on surface ozone and CO in eastern Asia.

[6] The studies as mentioned above basically focus on a certain long-range transport pathway and its impacts on air quality such as surface ozone level in the downwind regions. It is, however, necessary to systematically evaluate individual contributions of transport from various source regions in the globe including the remote troposphere as well as the industrialized regions to the global ozone and related species distributions and budgets, so that we can obtain a better perspective on future changes in ozone distributions. In this sense, the roles of interhemispheric exchange and vertical exchange of ozone and related species [*Staudt et al.*, 2001; *Lawrence et al.*, 2003a] should also be examined in detail.

[7] In this study, we systematically attribute global distribution and budget of tropospheric ozone to our defined source regions which cover the global atmosphere, using a tagged tracer simulation in the framework of the chemistry-climate transport model CHASER. The tagged tracer approach as introduced in the previous studies [*Wang et al.*, 1998a; *Bey et al.*, 2001; *Staudt et al.*, 2001; *Li et al.*, 2002a] provide a good perspective for transport from a selected source region and its influences on the global atmospheric composition. *Wild and Akimoto* [2001] have already studied impacts of transport from North America, Europe, and Asia on global ozone distribution in their perturbation simulation with 10% reduction of fossil fuel emissions. Our present study further investigates contributions from remaining source regions in detail as well, assessing absolute contributions from anthropogenic and natural sources in individual regions.

[8] Although in this study a tagged tracer for ozone does not differentiate between natural and anthropogenic sources, it is significant to investigate contributions of natural sources to ozone since natural emissions of precursors like lightning NO_x emissions may change in response to future climate change [*Price and Rind*, 1994]. For tagging O_3 tracers, we consider various regions in the planetary boundary layer (PBL) and free troposphere including both the industrialized and remote areas as origins of tropospheric ozone.

[9] This paper is going to discuss the roles of transport from various regions over the globe in O_3 distribution with highlighting characteristic long-range transport pathways as seen in this simulation. This kind of study also provides us with useful diagnostics of the performance of a chemistry transport model from which we can determine a possible cause of the model biases. We present the methodology including model description and experimental setup in section 2. Our simulated contributions from the defined source regions to the global distribution and budget of O_3 are discussed in section 3; this section also gives detailed discussions on the roles of long-range transport in the seasonal cycles and vertical profiles of O_3.

2. Methodology

[10] This study attempts to attribute global distribution and budget of tropospheric O_3 to various source regions in the global atmosphere. To isolate contributions from individual source regions, we use a tagged tracer method which was first introduced by *Wang et al.* [1998a, 1998b] and employed in several recent global model studies [*Bey et al.*, 2001; *Staudt et al.*, 2001; *Li et al.*, 2002a, 2002b]. The tagged tracer method treats a chemical species emitted or chemically produced in a certain region as a separate tracer and calculates its transport, chemical loss and surface deposition. This study performs a tagged tracer simulation using a chemistry-climate transport model CHASER [*Sudo et al.*, 2002a]. Details of the CHASER model and our tagged tracer simulation are described in the following.

2.1. Global Chemical Transport Model

[11] This study employs the coupled tropospheric chemistry climate model CHASER [*Sudo et al.*, 2002a] which has been developed in the framework of a GCM developed by the Center for Climate System Research (CCSR), the National Institute for Environment Studies (NIES), and the Frontier Research Center for Global Change (FRCGC) [*Numaguti*, 1993; *Numaguti et al.*, 1995; *Nozawa et al.*, 2005; *Nagashima et al.*, 2006]. For this study, the horizontal resolution of T42 ($2.8^\circ \times 2.8^\circ$) is adopted with 32 vertical layers from the surface to about 40 km altitude ($\sim$1 km vertical resolution in the upper troposphere and lower stratosphere, UTLS). The model considers a detailed online simulation of tropospheric chemistry involving O_3-HO_x-NO_x-CH_4-CO system and oxidation of nonmethane hydrocarbons (NMHCs) with a time step of 10 min, and includes detailed dry and wet deposition schemes also. The CHASER model version adopted in this study is basically identical to that described in *Sudo et al.* [2002a]. However, this version of CHASER, based on the CCSR/NIES/FRCGC GCM version 5.7, includes an improved wet deposition scheme, heterogeneous reactions on aerosols and cloud droplets for N_2O_5 and several radicals like HO_2, and an online simulation of sulfate as well. The implemented sulfate simulation

Table 1. Tracer Tagging With Different Sources for Ozone

Tracer ID	Source Region: Horizontal	Source Region: Vertical	Description
O_3-ALL	global	all	net (total) ozone
STRAT	global	stratosphere	transport from the stratosphere
TROPO[a]	global	troposphere	tropospheric chemical production
REMOT	remote[b]	troposphere	chemical production in remote regions
POLTD[c]	polluted	PBL[d] + FT[e]	chemical production in polluted regions
BL-AMN	see Figure 2a	PBL	PBL: North America
BL-AMM	see Figure 2a	PBL	PBL: Central America
BL-AMS	see Figure 2a	PBL	PBL: South America
BL-AFN	see Figure 2a	PBL	PBL: North Africa
BL-AFS	see Figure 2a	PBL	PBL: South Africa
BL-EUR	see Figure 2a	PBL	PBL: Europe
BL-CEU	see Figure 2a	PBL	PBL: Central Eurasia
BL-MES	see Figure 2a	PBL	PBL: Middle East
BL-IND	see Figure 2a	PBL	PBL: India etc.
BL-TLD	see Figure 2a	PBL	PBL: Thailand etc.
BL-CHN	see Figure 2a	PBL	PBL: China etc.
BL-JPN	see Figure 2a	PBL	PBL: Japan etc.
BL-IDN	see Figure 2a	PBL	PBL: Indonesia
BL-AUS	see Figure 2a	PBL	PBL: Australia
FT-AMN	see Figure 2b	FT	FT: North America
FT-AMS	see Figure 2b	FT	FT: South America
FT-AFN	see Figure 2b	FT	FT: North Africa
FT-AFS	see Figure 2b	FT	FT: South Africa
FT-EUR	see Figure 2b	FT	FT: Europe
FT-ASA	see Figure 2b	FT	FT: Asia
FT-IDN	see Figure 2b	FT	FT: Indonesia
FT-AUS	see Figure 2b	FT	FT: Australia

[a]Total chemical production in the troposphere defined as REMOT + POLTD.
[b]Remote region outside the POLTD regions (below 100 hPa altitude).
[c]Sum of O_3 tracers from the individual polluted regions as defined in Figure 2 (i.e., BL-AMN + BL-AMM + $\cdots$ + FT-AUS).
[d]Vertical regions of boundary layers (PBL) are defined as the six lowermost layers in the model (surface to approximately 750 hPa.
[e]Free troposphere (FT) is defined in the model to extend to 100 hPa altitude above PBL.

is linked to the heterogeneous reactions considered in the model, but not to the GCM's radiation component in this version. In CHASER, advective transport is simulated with a fourth-order flux-form advection scheme of the monotonic van Leer [*van Leer*, 1977] and the flux-form semi-Lagrangian scheme of *Lin and Rood* [1996]. Vertical transport associated with moist convection is simulated in the cumulus convection process in the GCM which is based on the Arakawa-Schubert scheme [*Emori et al.*, 2001]. The transport process in CHASER is evaluated by conducting a radon simulation in the work by *Sudo et al.* [2002a]. The model calculates the concentrations of 53 chemical species with 140 reactions (gas/liquid phase and heterogeneous). The concentrations of stratospheric O_3 and NO_y species above 55 hPa ($\sim$20 km) altitude are nudged to the monthly mean satellite data from the Halogen Occultation Experiment project (HALOE) [*Russel et al.*, 1993] and output data from the 3-D stratospheric chemistry model [*Takigawa et al.*, 1999] with a relaxation time of three days. In the detailed model evaluation [*Sudo et al.*, 2002b], good agreements between the CHASER simulations and observations are generally found for O_3 and precursor species including HO_x radicals. The CHASER model performance is also evaluated in the framework of the 4th assessment report of the Intergovernmental Panel on Climate Change (IPCC) [e.g., *van Noije et al.*, 2006].

[12] In this study, CHASER considers surface emissions for CO, NO_x, NMHCs, SO_2 and dimethyl sulfide as in *Sudo et al.* [2002a]. Anthropogenic emissions are basically prescribed by the Emission Database for Global Atmospheric Research (EDGAR) [*Olivier et al.*, 1996] Version 3.2 which provides global surface emissions for 1995. The distributions of biomass burning emissions are also specified by the EDGAR inventory with using the hot spots data derived by the Along Track Scanning Radiometer (ATSR) [*Arino et al.*, 1999] for simulating the seasonal variation of biomass burning emissions. The model includes natural NO_x sources from soils (5.5 TgN/yr) and lightning (5 TgN/yr) in this study. Biogenic emissions of NMHCs are identical to those given by *Sudo et al.* [2002a]: e.g., isoprene and terpenes emissions of 400 and 100 TgC/yr, respectively.

[13] In this study, we perform a climatological simulation. The CHASER model in this study is basically driven by the meteorological fields generated by the GCM, but moderately nudged to the data by the European Center for Medium-Range Weather Forecasts (ECMWF) for horizontal winds and temperatures in 1996 with a relaxation time of 7 days to reduce the GCM biases.

2.2. Tracer Tagging

[14] In this study, we transport separate O_3 tracers tagged by regions of origin in the framework of the CHASER model. The chemical tendency of O_3 produced in the region i is given as:

$$\frac{dQ_i(x,y,z)}{dt} = P_i(x,y,z) - \beta(x,y,z)\cdot Q_i(x,y,z) \qquad (1)$$

with Q_i the mixing ratio of O_3 tagged by the region i, β the chemical loss rate constant (s^{-1}), and P_i the gross chemical production within the region i.

$$P_i(x,y,z) = \begin{cases} P(x,y,z) & : \text{inside the region } i \\ 0 & : \text{outside the region } i \end{cases} \qquad (2)$$

Global fields of $\beta(x, y, z)$ and $P(x, y, z)$ are specified by 3-hourly output data from a standard full-chemistry run with CHASER. For $P(x, y, z)$, we use chemical production of the conventionally defined odd oxygen family O_x(= O_3 + O + $O(^1D)$ + NO_2 + $2NO_3$ + $3N_2O_5$ + PANs + HNO_3 + nitrates) instead of O_3 as in the works by *Wang et al.* [1998b] and *Li et al.* [2002a, 2002b]. *Li et al.* [2002a, 2002b] use their defined odd oxygen family as a substitute for O_3. As they state, O_3 accounts for more than 95% of such odd oxygen family on the global average. However, we found in our simulation that O_3 only accounts for 75 or 90% in the polluted boundary layers such as North America, Europe, and China. To remove this O_x induced error in O_3 calculation, we reduced above described chemical production P in the boundary layers as a function of the total concentration of NO_x and HNO_3 so that we can obtain good agreement with the O_3 concentrations calculated in the standard full-chemistry simulation. In addition to the chemical tendency, the model calculates the tendency due

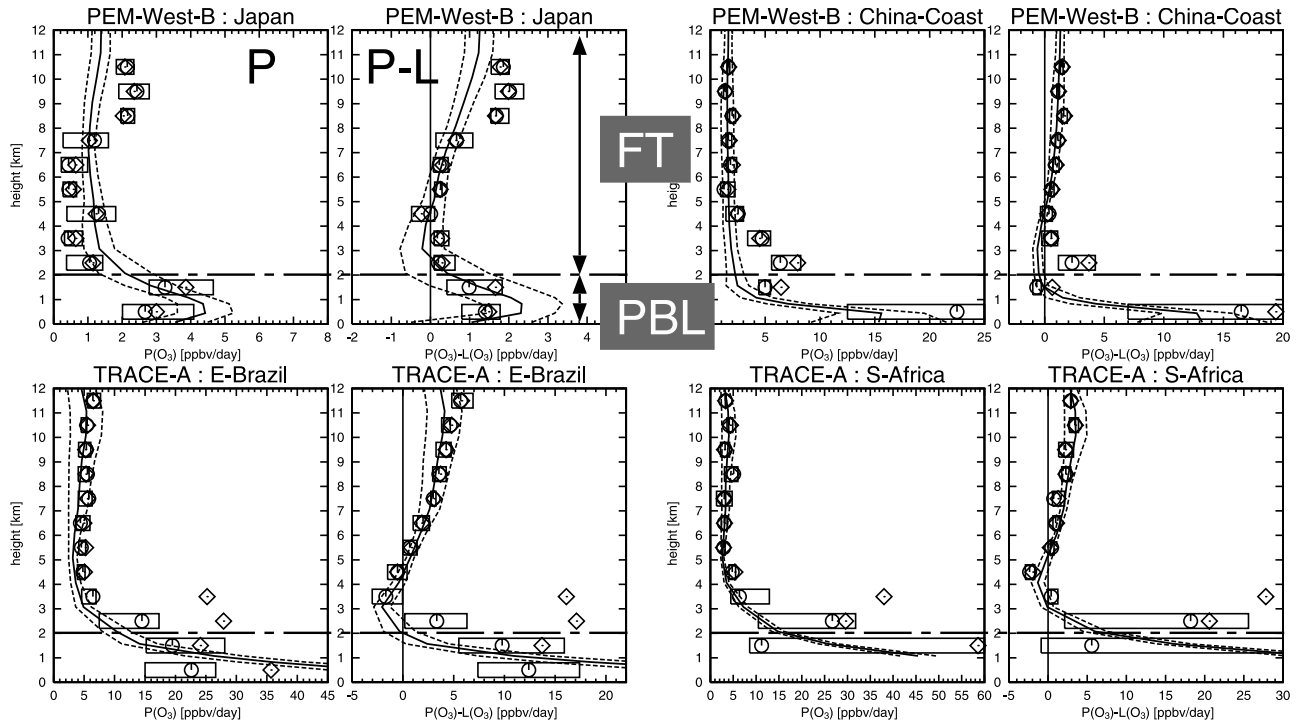

Figure 1. Vertical classification for O_3 tracer tagging based on vertical profiles of O_3 production $P(O_3)$ and net production $P\text{-}L(O_3)$ during the NASA Global Tropospheric Expedition (GTE) campaigns (PEM-West-B and TRACE-A). Solid and dashed lines show temporal mean and $\pm\sigma$ of the CHASER model calculation, respectively. The observations show mean (diamonds), median (circles), and inner 50% of the data (boxes) for the NASA GTE campaigns.

to transport and dry deposition at the surface for each O_3 tracer.

[15] Using tagged tracers as described above, we classify O_3 by various source regions as shown in Table 1. First the total O_3 (O_3-ALL) is separated into the stratospheric origin (STRAT) and tropospheric origin (TROPO). In this study, TROPO is defined as the sum of the O_3 tracers tagged by chemical production in the remote region (REMOT) and polluted region (POLTD) in the troposphere. To further separate polluted source region POLTD, we first consider vertical classification based on the profiles of O_3 production in the polluted regions as seen in Figure 1. The net O_3 production derived from observations and calculated by the model is much intense within the planetary boundary layers (PBL) with a rapid decrease with altitude (negative or near zero values slightly above the PBL) and an increase in the free troposphere (1–5 ppbv/day in the upper troposphere). This sort of vertical profile of net O_3 production indicates that the O_3 production process in the polluted regions can be separated into two different regimes: production in the PBL and in the free troposphere (FT). Moreover, in the CHASER model the global amounts of O_3 production in the lower troposphere (including PBL) and free troposphere are estimated to be well comparable with each other (2266 and 2478 TgO_3/yr, respectively) as other model studies [e.g., *Horowitz et al.*, 2003]. We, therefore, investigate contributions from the polluted region (POLTD) with distinction between PBL and free troposphere. In this study, we differently separate horizontal regions in the PBL and free troposphere in view of the distributions of O_3 production (Figure 2): 14 regions in the PBL (defined as the six lowermost layers in the model, surface to ~750 hPa) and 8 regions in the free troposphere. The O_3 tracer of stratospheric origin (STRAT) is calculated by setting it equal to total O_3 (O_3-ALL) in the stratosphere at each time step. In many of the previous studies [e.g., *Follows and Austin*, 1992; *Roelofs and Lelieveld*, 1997; *von Kuhlmann et al.*, 2003], such fixing of a stratospheric O_3 tracer is considered just above the tropopause as defined with the lapse rate or O_3 concentration of ~150 ppbv. We, however, found a large contribution of tropospheric origin to O_3 levels in the lowermost stratosphere near the tropopause in our CHASER simulations, indicating a non negligible flux of O_3 and its precursors (especially NO_x) from the troposphere to the lower stratosphere as associated with deep convection [*Fischer et al.*, 2002]. We, therefore, scale the STRAT O_3 tracer to the total O_3 only above 100 hPa altitude in the model to investigate a pure contribution from the stratosphere.

[16] In this study, we also transport separate CO tracers tagged by CO emissions over the same regions as for the PBL O_3 tracers (Figure 2a) to diagnose transport from the individual source regions.

[17] Tagged tracer method as used in this study can provide contributions from various source regions with a reasonable computational efficiency. We, however, need to note several features of this method especially for O_3. First a tagged tracer for a certain region *i* does not include a contribution from O_3 production outside the region associated with outflow of precursors originating in the region *i*, but can include O_3 production associated with inflow of

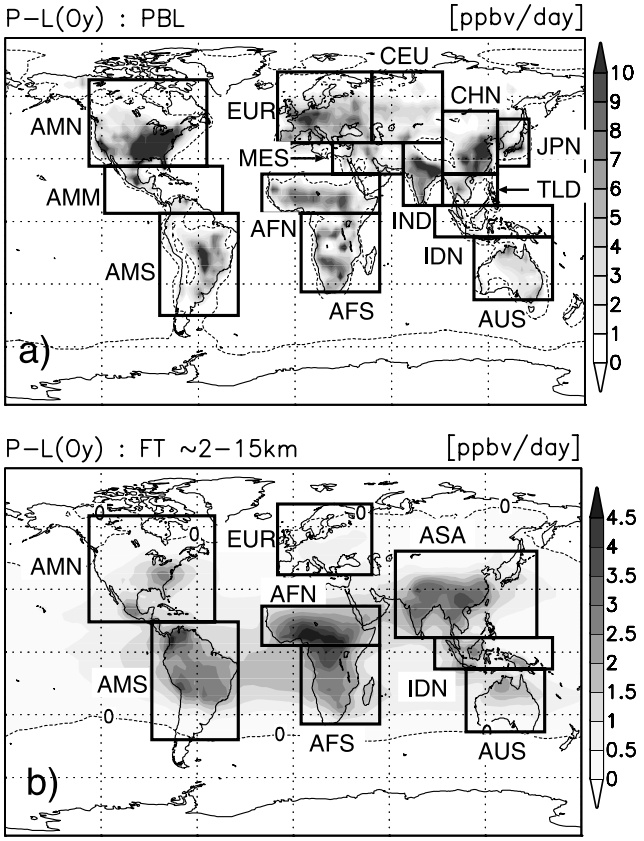

Figure 2. Regional separation for tracer tagging with distributions of the net O_3 production (annual mean) calculated by CHASER in (a) PBL and (b) free troposphere (FT). The defined POLTD source regions occupy 33% of the Earth's surface area in PBL and 32% in FT.

precursors originating in other regions. In this sense, our tagged O_3 tracers may underestimate or overestimate actual contributions from the individual selected regions shown in Figure 2. However, such interregional transport (inflow/outflow) of precursors can be estimated to have little impact on O_3 production within the individual polluted regions particularly in the PBL, since chemical lifetime of NO_x the predominant key precursor of O_3 is typically a few hours or a day in the PBL, much shorter than timescale of interregional transport. On the other hand, interregional transport of NO_x is more possible in the free troposphere because of longer lifetime of NO_x and NO_x recycling from reservoir species like PAN [*Fan et al.*, 1994; *Moxim et al.*, 1996]. We therefore selected relatively large horizontal regions for tagging free tropospheric O_3 production as in Figure 2b; however, it should be still noted that FT O_3 tracers can neglect interregional influences as associated with PAN transport in the cold upper troposphere.

[18] This study evaluates contributions from remote O_3 production outside the defined polluted regions (as associated with long-range export of precursors) with an O_3 tracer tagged by production in the remote areas (REMOT). Another notifiable feature of a tagged tracer is that it does not differentiate between anthropogenic origins and natural origins as coming from NO_x emissions from lightning or soils and biogenic NMHCs emissions from vegetation. As previous model studies investigated [e.g., *Berntsen et al.*, 1997; *Mickley et al.*, 1999], anthropogenic emissions of O_3 precursors are considered to contribute largely to O_3 levels in the free troposphere as well as in the PBL. Our CHASER simulations of preindustrial and present-day tropospheric O_3 (separate work from this study) indicate that anthropogenic emissions of O_3 precursors account for more than 80% of the gross O_3 production in the polluted PBL in the NH (i.e., North America, Europe, and East Asia) and for around 50% in the continental PBL in the tropics and the SH (i.e., South America, Africa, Australia, etc.). In the free troposphere, anthropogenic impacts on O_3 production can be expected to be less discernible because of limited injection of anthropogenic precursors from the surface and larger contributions from lightning NO_x. Our simulations show that anthropogenic emissions explain about 70% of free tropospheric gross O_3 production in North America, Europe, and East Asia, but only 20–30% in other continental regions such as South America, Africa, and Australia reflecting large natural contributions from lightning NO_x and biogenic NMHCs emissions. In view of these profiles of anthropogenic contributions to O_3 production, we concluded that our O_3 tracers tagged by the polluted regions in the NH generally provide a good perspective for anthropogenic impacts in the

Table 2. NASA GTE Campaign Regions and Dates

Campaign	Dates	Region Name[a]	Latitudes	Longitudes
ABLE-3B	6 Jul to 15 Aug 1990	Ontario	45–60°N	270–280°E
SONEX	7 Oct to 12 Nov 1997	Atlantic	35–45°N	325–345°E
PEM-WEST-A	16 Sep to 21 Oct 1991	Hawaii	15–35°N	180–210°E
PEM-WEST-B	7 Feb to 14 Mar 1994	Philippine-Sea	5–20°N	135–150°E
PEM-Tropics-A	15 Aug to 5 Oct 1996	Chris.-Island	0–10°N	200–220°E
		Tahiti	20°S–0°	200–230°E
		Fiji	30–10°S	170–190°E
		Easter-Island	40–20°S	240–260°E
PEM-Tropics-B	6 Mar to 18 Apr 1999	Hawaii	10–30°N	190–210°E
		Tahiti	20°S–0°	200–230°E
TRACE-A	21 Sep to 26 Oct 1992	S-Africa	25–5°S	15–35°E
		W-Africa-Coast	25–5°S	0–10°E
		S-Atlantic	20°S-0°	340–350°E
		E-Brazil	15–5°S	310–320°E
TRACE-P	3 Mar to 15 Apr 2001	Japan	25–40°N	135–150°N
		China-Coast	20–30°N	115–130°E

[a]Listed only for regions used in this study.

NH as suggested by *Li et al.* [2002b], though those tagged by other regions (mostly in the SH) may contain a large contribution from natural emissions as well.

3. Results and Discussions

3.1. Horizontal Distributions

[19] Before discussing contributions from the individual source regions, we first compare the tropospheric O_3 (total) distributions simulated in this study with the tropospheric ozone residual (TOR) data [*Fishman et al.*, 2003] which are derived from the total column O_3 measured by the Total Ozone Mapping Spectrometer (TOMS) and stratospheric column O_3 by the Stratospheric Aerosol and Gas Experiment (SAGE) instrument in Figure 3. Our calculation generally captures the TOR derived O_3 distributions well. It reproduces springtime O_3 enhancements reaching 40 DU in the northern midlatitudes including the eastern Asia and Pacific, and summer O_3 peaks (40–50 DU) in the United States (U.S.), Middle East, and East Asia. The calculated summertime O_3 abundances in East Asia appear to be smaller than the TOR measurements (especially in China), maybe reflecting an underestimation of recent O_3 precursors emissions in China in the model; the emission data used in this study are basically for 1995, whereas the TOR measurements shown in Figure 3 are for 1998 to 2001. In October, CHASER well replicates biomass burning induced O_3 enhancements in South America, Atlantic, and South Africa as observed by the TOR, reproducing high O_3 abundances (>40 DU) over the Atlantic and Indian Ocean that reach the western coast of Australia. The O_3 levels in the Atlantic and North Africa, however, appear to be 10–20% overestimated by CHASER all the year round. Evaluation of spatial and temporal distributions of O_3 is also presented in sections 3.2 and 3.3.

[20] Using our defined tagged tracers, we first separate tropospheric column O_3 into tropospheric and stratospheric origins as shown in Figure 4. O_3 from tropospheric chemical production (TROPO) shows much larger contributions than that from stratosphere (STRAT) giving an inhomogeneous pattern in the horizontal distribution with strong O_3 peaks (>35 DU) around East Asia, Middle East to India, and South Atlantic. On the other hand, O_3 of stratospheric origin (STRAT) shows zonally uniformal contributions of around 10 DU in the extratropics and 2–5 DU in the tropics. STRAT explains only 10–20% of total tropospheric column O_3 in the tropics and 20–30% in the northern midlatitudes, but has contributions comparable with tropospheric origin (TROPO) in the southern high latitudes. At the surface elevation, annual mean STRAT O_3 concentrations are calculated to be 1–4 ppbv (5–20% of total O_3) in the tropics and 5–8 ppbv (20–25%) in the extratropics in the NH (~5 ppbv in the SH). In the polluted regions in the NH like North America and Europe, we calculate very small STRAT contributions of around 10% on the annual average with larger contributions from chemical O_3 production (see also discussions in sections 3.2 and 3.3). These estimated stratospheric contributions to tropospheric O_3 appear much smaller than those estimated by several of the previous global model studies [e.g., *Roelofs and Lelieveld*, 1997; *von Kuhlmann et al.*, 2003], but consistent with *Follows and Austin* [1992] and *Wang et al.* [1998c]. This can be attributed to the difference in definition of a stratospheric O_3 tracer. Figure 4 also compares O_3 contributions from chemical production in the polluted (POLTD) and remote (REMOT) regions as two distinct components of the TROPO contribution. In the polluted continental regions POLTD O_3 largely contributes to TROPO by 20–30 DU, but inflow of remote O_3 from the remote regions (REMOT) also has a significant contribution of 5–10 DU there. It should be noted that REMOT O_3 has a contribution comparable with POLTD O_3 in the remote regions especially in the high latitudes in the both hemispheres, indicating a significance of O_3 precursors outflow from the continental polluted regions to remote regions (mostly oceanic regions) and subsequent O_3 production there. A REMOT O_3 peak (~15 DU) is seen in the southern Atlantic, associated with outflow of natural and anthropogenic precursors from South America and Africa, and with NO_x recycling from PANs [*Sudo et al.*, 2002b]; this REMOT O_3 peak appears to be responsible for the South Atlantic O_3 maximum as in Figure 4a.

[21] In Figure 5, the POLTD column O_3 is further segregated into contributions from the individual source regions defined for the free troposphere (FT) and PBL (BL) in Table 1. The free tropospheric contributions (FT tracers) are generally larger and more extensive than the PBL ones (BL tracers) because of longer photochemical/residential lifetime of O_3 (see Table 3) and faster horizontal transport in the free troposphere. O_3 from North American free troposphere (FT-AMN) has a contribution larger than 1 DU through much of the NH. A peak contribution from FT-AMN, calculated around the source region (~5 DU on an annual average), ranges from 2–3 DU in winter to ~15 DU in summer; as *Cooper et al.* [2006] showed, lightning NO_x production over North America can contribute significantly to the summertime FT-AMN O_3 enhancements in the free troposphere. Significant export of FT-AMN O_3 is seen in the northern Atlantic (5–10 DU) in summer, extending to the Mediterranean and Middle East (3–4 DU) as *Li et al.* [2002b] suggested. However, hemispheric impact from FT-AMN is calculated to be the most significant in October when O_3 lifetime becomes longer (see discussions below). The largest contribution to O_3 in the NH appears to come from the Asian free troposphere (FT-ASA). In the course of a year, the peak contribution from FT-ASA seen around Asia increases from 4–5 DU in winter to 17–20 DU in summer in the same manner as FT-AMN O_3. From July through October, our model calculates significant O_3 outflow (~10 DU) from the FT-ASA region toward the Pacific and North Africa (via Middle East). As studied by *Li et al.* [2001], O_3 exports from FT-AMN and FT-ASA both contribute to the column O_3 peak calculated in Middle East in summer as seen in Figure 4c. FT-ASA O_3 also appears to have a nonnegligible contribution even in the SH. In the SH midlatitudes, contributions from the South American and African free troposphere (FT-AMS and FT-AFS) are the most significant owing to enhanced O_3 production with abundant precursors from biomass burning, vegetation, and lightning in those regions; both contributions show similar export pathways (>2 DU) over the Indian Ocean toward Australia and the Pacific as shown by *Chatfield et al.* [2002] and *Piketh et al.* [2002]. It should be noted that O_3 transport from South America (FT-AMS) has another branching

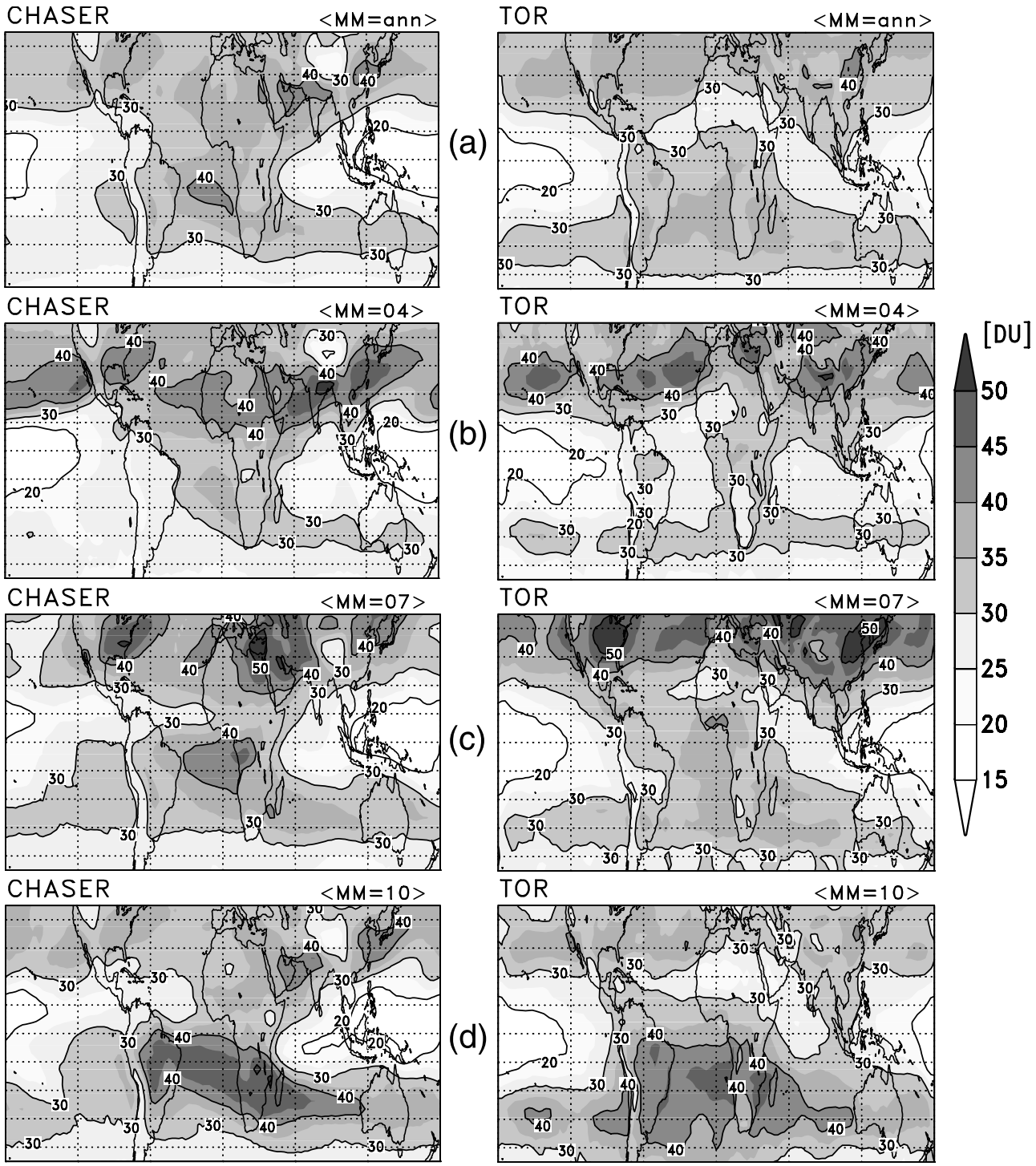

Figure 3. Tropospheric column ozone distributions (left) calculated by CHASER and (right) derived from satellite data with the Tropospheric Ozone Residual (TOR) method [*Fishman et al.*, 2003], shown for (a) annual mean, (b) April, (c) July, and (d) October. The TOR measurements show averages during 1998 to 2001.

pathway extending in the NH toward Asia. Column O_3 from two African regions (FT-AFN and FT-AFS), under the influence of the Harmattan wind and Walker circulation [*Thompson et al.*, 2000, 2001; *Edwards et al.*, 2003], shows peaks ($\sim$10 DU) outside those regions in the Atlantic. In comparison with these free tropospheric contributions, contributions from PBL O_3 production (BL tracers) to column O_3 amounts are much confined within the individual source regions by shorter chemical lifetime and surface dry deposition of O_3. We, however, note that hemispheric contributions from PBL regions in North America and Europe (BL-AMN and BL-EUR) are well comparable with those from free

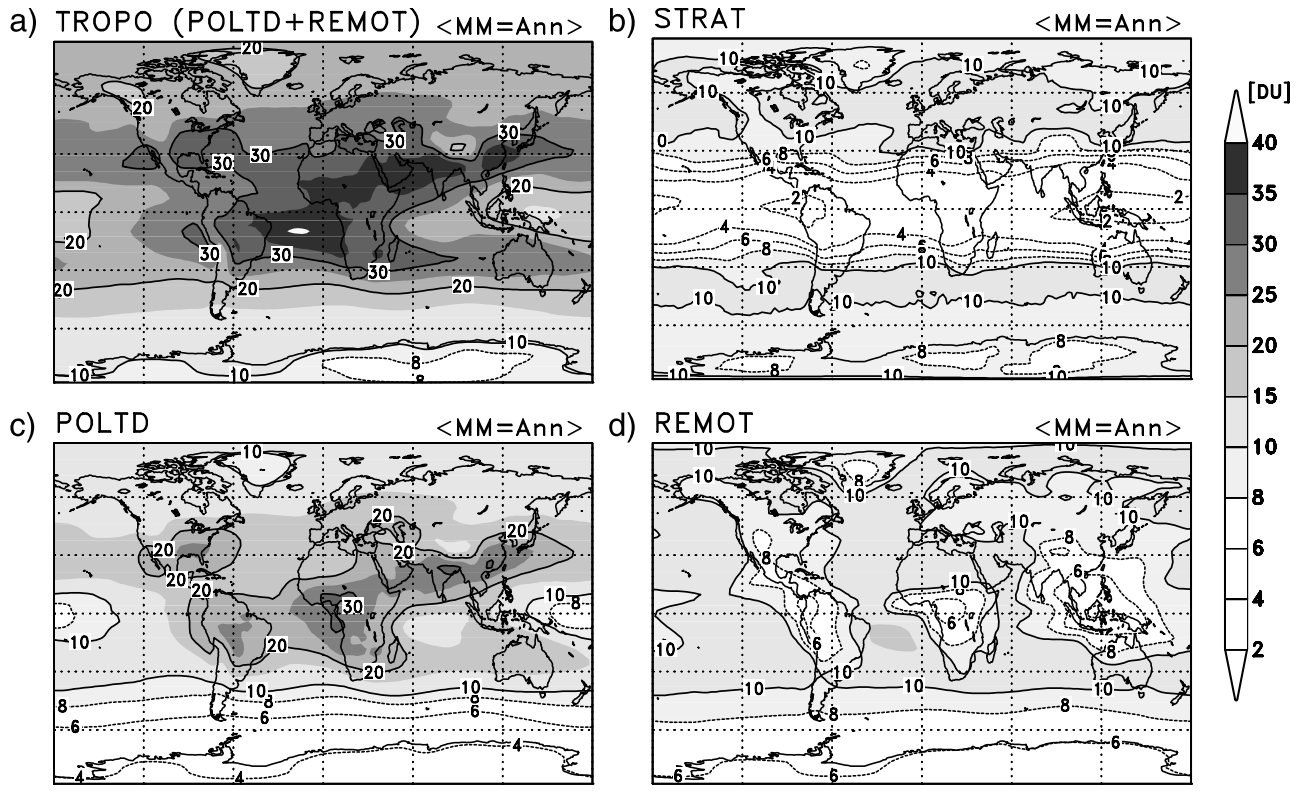

Figure 4. Contributions to annual mean tropospheric column ozone from (a) total chemical production in the troposphere (TROPO) defined as POLTD + REMOT, (b) transport from the stratosphere, (c) chemical production in the polluted regions (POLTD), and (d) chemical production in the remote regions (REMOT). See Table 1 for detailed description of source classification.

troposphere in the same regions (FT-AMN and FT-EUR). Long-range transport from PBL in the China region (BL-CHN) also gives large hemispheric contribution (~1 DU) in spite of its much small horizontal area relative to BL-AMN and BL-EUR (see Figure 2a). Unlike BL-CHN, contributions from PBL regions in other Asian regions such as BL-IND and BL-TLD are quite limited in the vicinity of those source regions because of a shorter chemical lifetime of O_3. In the SH, our model calculates large contributions (>1 DU) from PBLs in South America and Africa (BL-AMS and BL-AFS) extending toward Australia like O_3 export pathways from FT-AMS and FT-AFS.

[22] We also examined contributions from the individual POLTD regions to O_3 in PBL in the context of global air quality. As can be expected, contributions from PBL O_3 production (BL tracers) are generally much larger than those from free tropospheric production (FT tracers). Particularly, O_3 from PBL in the North America, Europe, central Eurasia, and China regions appears to have a hemispheric distribution (Figure 6). These long-range O_3 exports are the most significant in spring or autumn when relatively large chemical production and long lifetime of O_3 coexist; e.g., the BL-AMN O_3 at the surface in Europe peaks in April and October (2–6 ppbv) in agreement with the study by *Auvray and Bey* [2005] (see also discussions in section 3.2). O_3 transport from the European PBL (BL-EUR) reaches the eastern Asia including Japan along the Trans-Eurasian transport pathway in winter to spring (2–2.5 ppbv), comparable with *Liu et al.* [2002] and *Wild et al.* [2004].

[23] Export from the Chinese PBL (BL-CHN) appears to have a large contribution to O_3 levels in the remote Pacific and U.S. in spring and autumn (2–3 ppbv in April/October). In April, the Asian O_3 tracers, BL-CHN, BL-TLD, BL-IND, and BL-JPN, amount to about 3.5 ppbv at the surface in the western U.S., comparable with the estimates by *Berntsen et al.* [1999] and *Yienger et al.* [2000].

[24] We also found large contributions from several free tropospheric regions to PBL O_3 linked to downward motion associated with a high-pressure system and convection [e.g., *Lawrence et al.*, 2003a].

[25] O_3 from the Asian free troposphere (FT-ASA), having a large contributions in the NH, shows an extensive peak (3–10 ppbv) in the PBL in Southeast Asia and western Pacific in summer (see also section 3.2). This can be attributed to the combined effect of lightning NO_x emissions and downward O_3 transport associated with monsoon related convective activities in these regions [e.g., *Ma et al.*, 2002]. Transport from Asia (FT-ASA) in summer (JJA) also affects surface O_3 in the U.S. showing a peak of 2–4 ppbv in the western U.S. Although FT-ASA O_3 may contain natural components as associated with lightning NO_x in addition to anthropogenic ones, the FT-ASA O_3 concentrations at the U.S. surface in summer appear to be comparable with the impacts of Asian anthropogenic emissions on the U.S. O_3 calculated by *Li et al.* [2002b].

[26] O_3 from the free troposphere in North America (FT-AMN) also has large contributions (>1 ppbv in annual mean) in the NH in the same magnitude as BL-AMN O_3

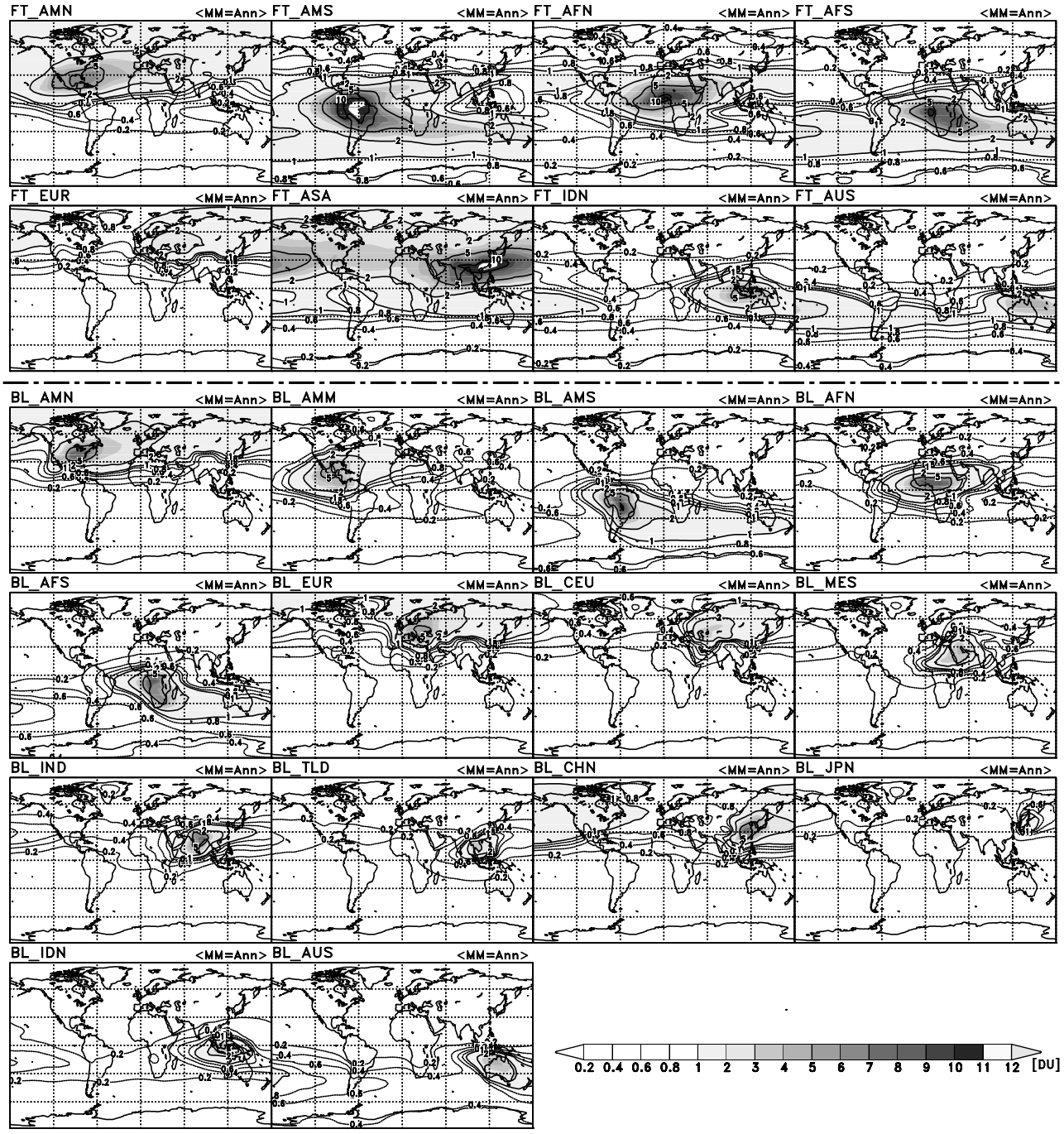

Figure 5. Tropospheric column ozone from the polluted (POLTD) regions (annual mean), composed of 8 free tropospheric (FT) regions and 14 PBL (BL) regions (see Table 1 for region definition).

(not shown). In summer, FT-AMN O_3 shows a peak of 2–3 ppbv at the surface around Middle East reflecting subsidence there, which is in line with *Li et al.* [2002b].

[27] Long-range O_3 transport in the upper troposphere from individual source regions is also evaluated as in Figure 7 for 8 km altitude. Exports from FT-AMN and FT-ASA have a particularly large contribution for the NH O_3 at this altitude. The FT-AMN O_3 peak over the U.S. and North Atlantic, larger than 10 ppbv in annual mean, is the most significant in July reaching ~30 ppbv. Similarly, the FT-ASA O_3 peak around Southeast Asia reaches its maximum (40 ppbv) in July, leading to long-range O_3 transport (>10 ppbv) to the U.S.; the FT-ASA contribution to the U.S. O_3 at this altitude is constantly seen almost all year round. We also found a large contribution from FT-ASA to the SH O_3 which is most clearly seen in June–September. In this season, O_3 produced in the Asian free troposphere is efficiently conveyed by an easterly current in the upper troposphere associated with the anticyclonic circulation centering around the Tibetan plateau [*Barry and Chorley*, 2003; *Auvray and Bey*, 2005]. Over the western Indian Ocean, Africa, and Atlantic, this upper tropospheric stream

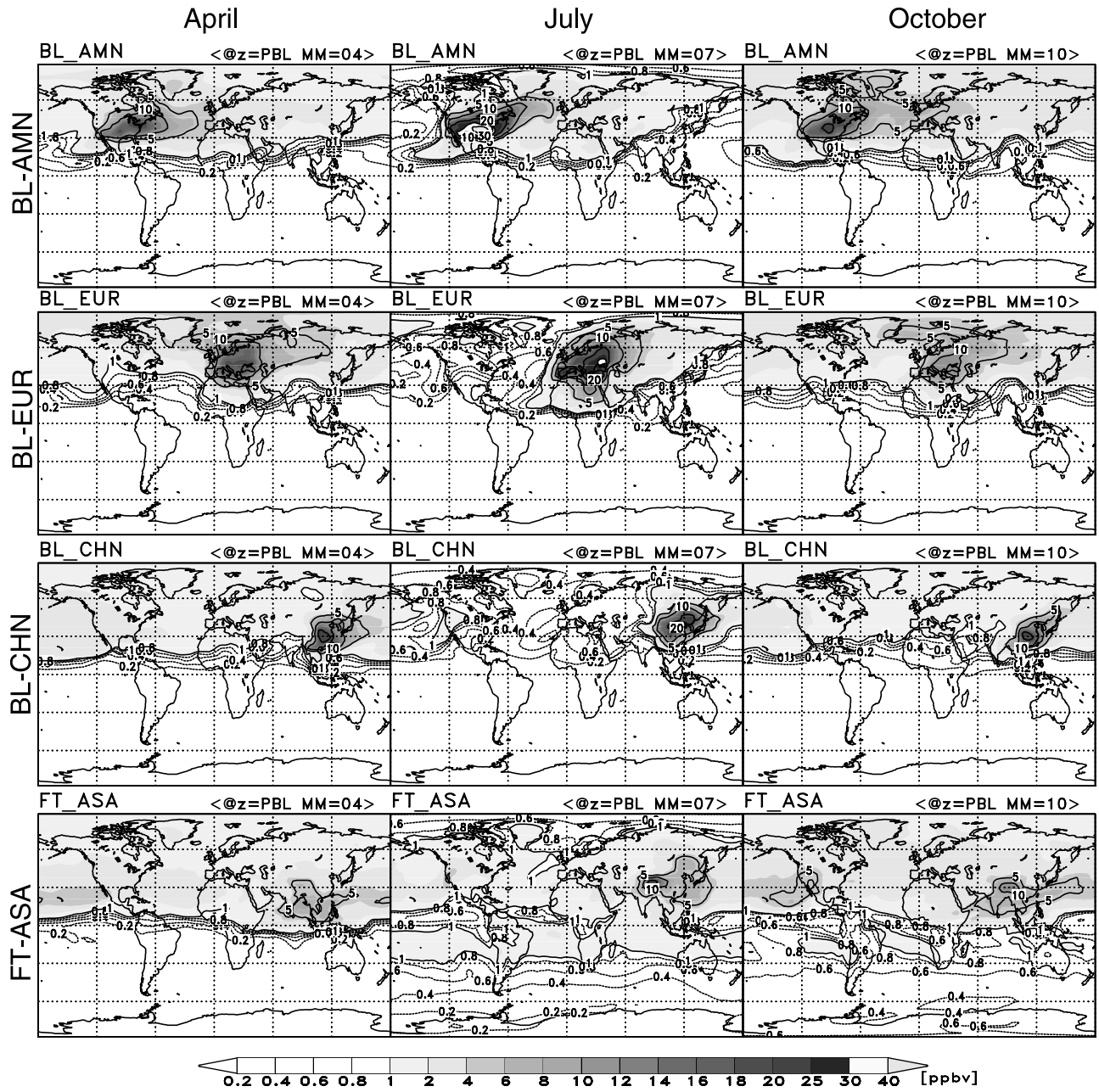

Figure 6. PBL mean mixing ratios for selected tagged O_3 tracers for April, July, and October: BL-AMN, BL-EUR, BL-CHN, and FT-ASA (see Table 1 for region definition).

of O_3 branches out to two directions: one toward Middle East and Europe [*Auvray and Bey*, 2005; *Lawrence et al.*, 2003b], and the other toward the SH. The branch toward the SH imports Asian O_3 into the southern midlatitudes toward Australia in conjunction with the westerly jet in the SH; the model calculates a large FT-ASA contribution (>5 ppbv) at 8 km over Australia in July. The model study by *Staudt et al.* [2001] showed a similar upper tropospheric cross-equatorial transport of Asian fossil fuel CO to the southern midlatitudes via the Indian Ocean and Atlantic. The FT-ASA contribution to the middle-upper tropospheric O_3 in the southern midlatitudes is also discussed in section 3.2 and 3.3. Our simulation also revealed that export from FT-AMS (South America) has a pathway toward the eastern Asia to the North Pacific joining export pathway from FT-AFN (North Africa). These O_3 outflows from FT-AMS and FT-AFN to the northern midlatitudes, most clearly seen during January to April, play an important role in the seasonal variation and vertical profile of O_3 in Asia and North Pacific (see section 3.2). Our model also calculates relatively large contributions from O_3 production in PBL (BL tracers) to O_3 at 8 km altitude: e.g., ~2 ppbv annual contributions from each of BL-AMN and BL-CHN in the NH, which are caused by uplifting associated with the warm/cold conveyor belt in midlatitude cyclones [*Browning and Roberts*, 1994; *Hannan et al.*, 2003] and by convective updraft in the low-mid latitudes [*Lawrence et al.*, 2003a].

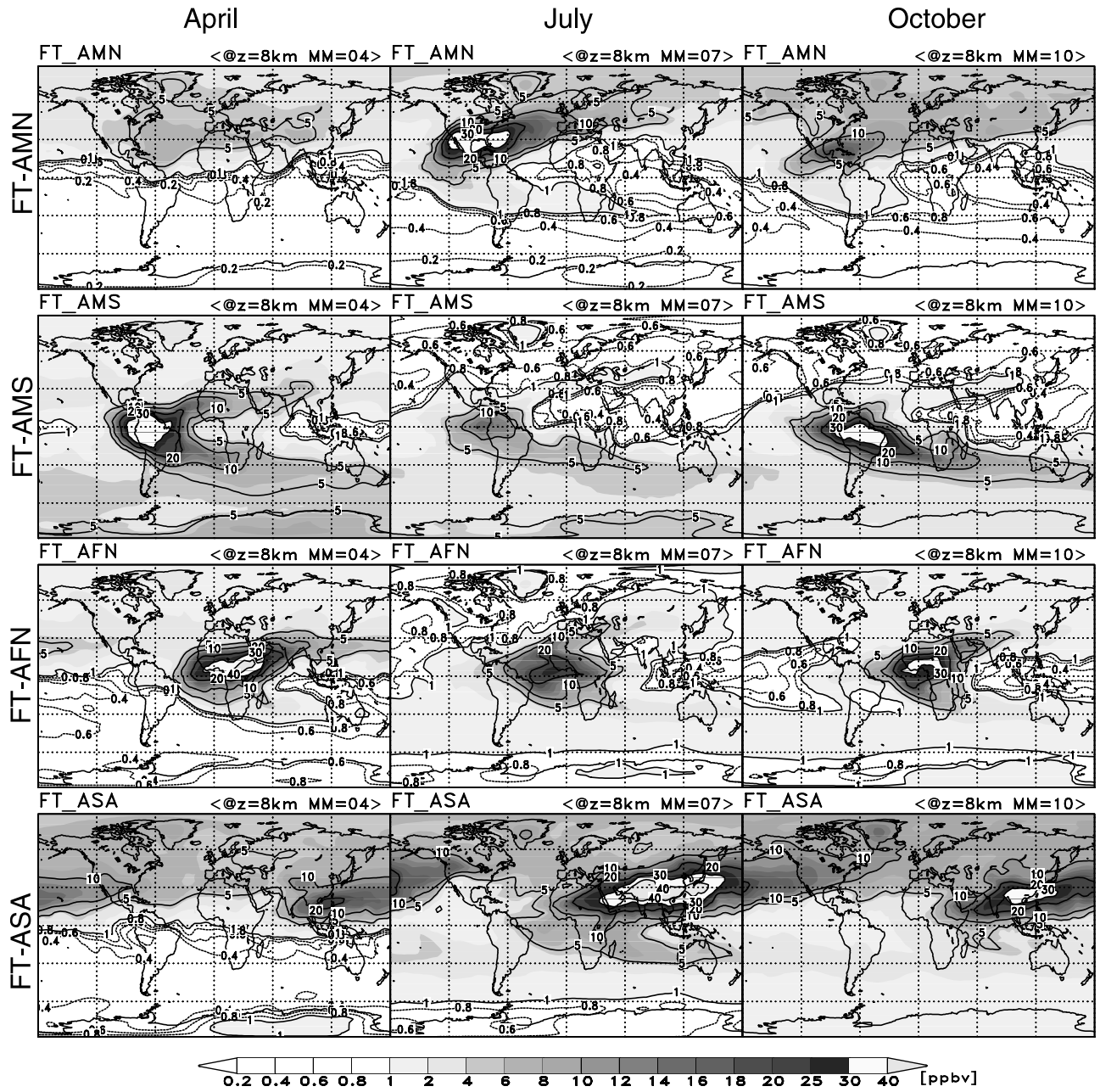

Figure 7. Distributions of selected tagged O_3 tracers at 8 km altitude for April, July, and October: FT-AMN, FT-AMS, FT-AFN, and FT-ASA (see Table 1 for region definition).

3.2. Seasonal Variations

[28] In this section, we evaluate contributions from individual source regions (STRAT, REMOT, and POLTD regions) to seasonal variation of tropospheric O_3. Figure 8 gives contributions from the individual source regions defined in Table 1 to O_3 seasonal variations at the three remote surface sites. Tropospheric and stratospheric origins both contribute to O_3 seasonality at these sites. At Mace Head, in winter and spring, 50–60% of O_3 level is explained by O_3 transport from the polluted regions (POLTD) with ~30% imported from the remote region (REMOT). In summer, the POLTD contribution at Mace Head decreases to ~25%, but instead the REMOT contribution increase to 60–70%, reflecting less efficient long-range transport from the polluted regions and more enhanced chemical O_3 production in the remote atmospheres (particularly in the Atlantic). The lower panel, focusing on the POLTD contributions, shows the largest contributions from the BL-EUR and BL-AMN (2–10 ppbv). The BL-EUR and BL-AMN O_3 concentrations at Mace Head appear to negatively correlate in time with each other, reflecting wind pattern changes over the Atlantic due to temporal variability in the Atlantic high-pressure system. It should be noted that in fact there is interannual variability in transport from North America to Europe associated with the North Atlantic Oscillation (NAO) as well [*Li et al.*, 2002b]. There appears to be a significant long-range transport of O_3 from Asia (FT-ASA and BL-CHN) to Mace Head especially in nonsummer seasons (1–3 ppbv) which is also seen in the

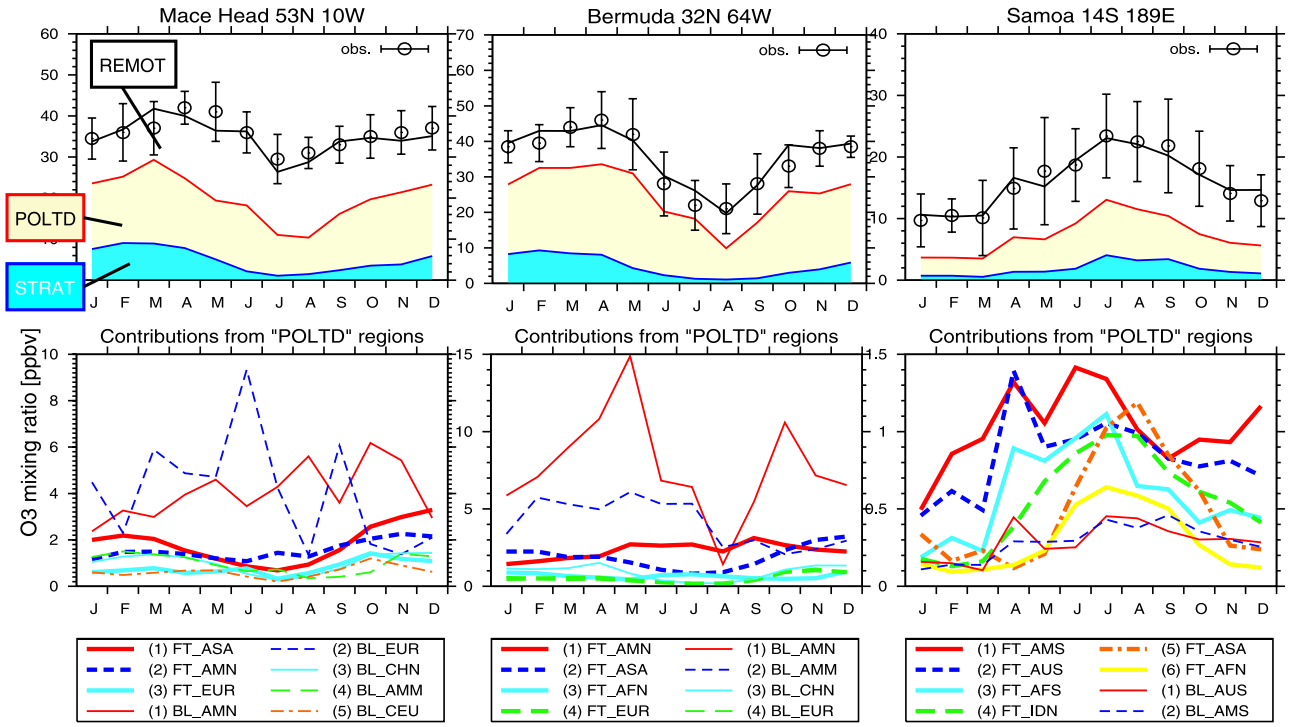

Figure 8. Observed and calculated seasonal variations of O_3 at three surface sites with contributions from stratospheric O_3 transport (STRAT), O_3 production in the polluted regions (POLTD), and remote regions (REMOT). In the bottom plots, the top eight contributions of the POLTD regions are shown; key labels are sorted by PBL (BL) and free tropospheric (FT) contributions separately. The observations show climatology taken from *Logan* [1999].

previous model studies [*Derwent et al.*, 2004; *Auvray and Bey*, 2005].

[29] At Bermuda, O_3 seasonal variation is mostly controlled by POLTD O_3 rather than REMOT O_3 which is constant through the year. Transport from PBL in North and central America (BL-AMN and BL-AMM) gives the largest contributions with spring peaks of 15 and 6 ppbv, respectively. O_3 transport from these PBL regions is, however, strongly inhibited in summer going down to ~1 ppbv in August, and instead transport from the free troposphere in North America (FT-AMN) increases in summer. The dominant contribution from North American PBL (BL-AMN) to spring O_3 at Bermuda in this study is in line with the model study by *Li et al.* [2002a] which also suggests the primary importance of continental outflow from North America for springtime O_3 at Bermuda. Contributions from Asia (FT-ASA and BL-CHN) are also seen particularly in winter to spring (1–3 ppbv). In the case of Samoa, a remote site in the South Pacific, seasonal variation of O_3 is explained by the combination of transport from the REMOT, POLTD, and STRAT regions. Contributions from various source regions in the SH and tropics are jumbled in the lower panel. It is remarkable that O_3 from the Asian free troposphere (FT-ASA) gives a large contribution (>1 ppbv) from July through September together with FT-AFN O_3, resulting from the interhemispheric transport pathway from Asia via Africa to the southern midlatitudes as already described in the previous section.

[30] Similarly, Figure 9 shows contributions from the individual source regions to O_3 seasonalities at distinct altitudes (800, 500, and 300 hPa). At Resolute, 800 and 500 hPa O_3 concentrations in summer are largely controlled by REMOT O_3 (60–70%) which mainly reflects O_3 production in the North Pacific, Atlantic, and Arctic areas. POLTD O_3, however, gives important contributions to 800/500 hPa O_3 in nonsummer seasons, showing large O_3 imports (1–5 ppbv) from the free troposphere and PBL in North/central America, Asia, Europe, and central Eurasia. At 300 hPa, stratospheric O_3 (STRAT) dominantly controls the O_3 seasonality, but O_3 of tropospheric origin (POLTD + REMOT) also gives an important contribution (30–50%) with high concentrations (6–10 ppbv) of O_3 from the Asian free troposphere (FT-ASA). At Höhenpeissenberg, a European site, seasonal variation of 800 hPa O_3 is explained mostly by O_3 production in the European PBL (BL-EUR) as can be expected. There are, however, nonnegligible contributions from North America and Asia (BL/FT-AMN and FT-ASA) ranging from 1 to 5 ppbv, which are comparable with *Derwent et al.* [2004] and *Auvray and Bey* [2005].

[31] In contrast to 800 hPa O_3, 500 and 300 hPa O_3 seasonal variations show a mixture of O_3 contributions from the North American and European regions (FT/BL-AMN and FT/BL-EUR) in the same magnitude which increase in summer. Import of Asian O_3 (FT-ASA and BL-CHN) is clearly seen at these free tropospheric altitudes with a high concentration of FT-ASA O_3 increasing from summer to autumn consistent with *Auvray and Bey* [2005]. The model also shows a relatively constant contribution (1–2 ppbv) from North Africa (FT-AFN).

[32] At Sapporo and Kagoshima Japan, located in the eastern edge of Asia, O_3 seasonal variation at every altitude is largely influenced by O_3 production in the Asian free

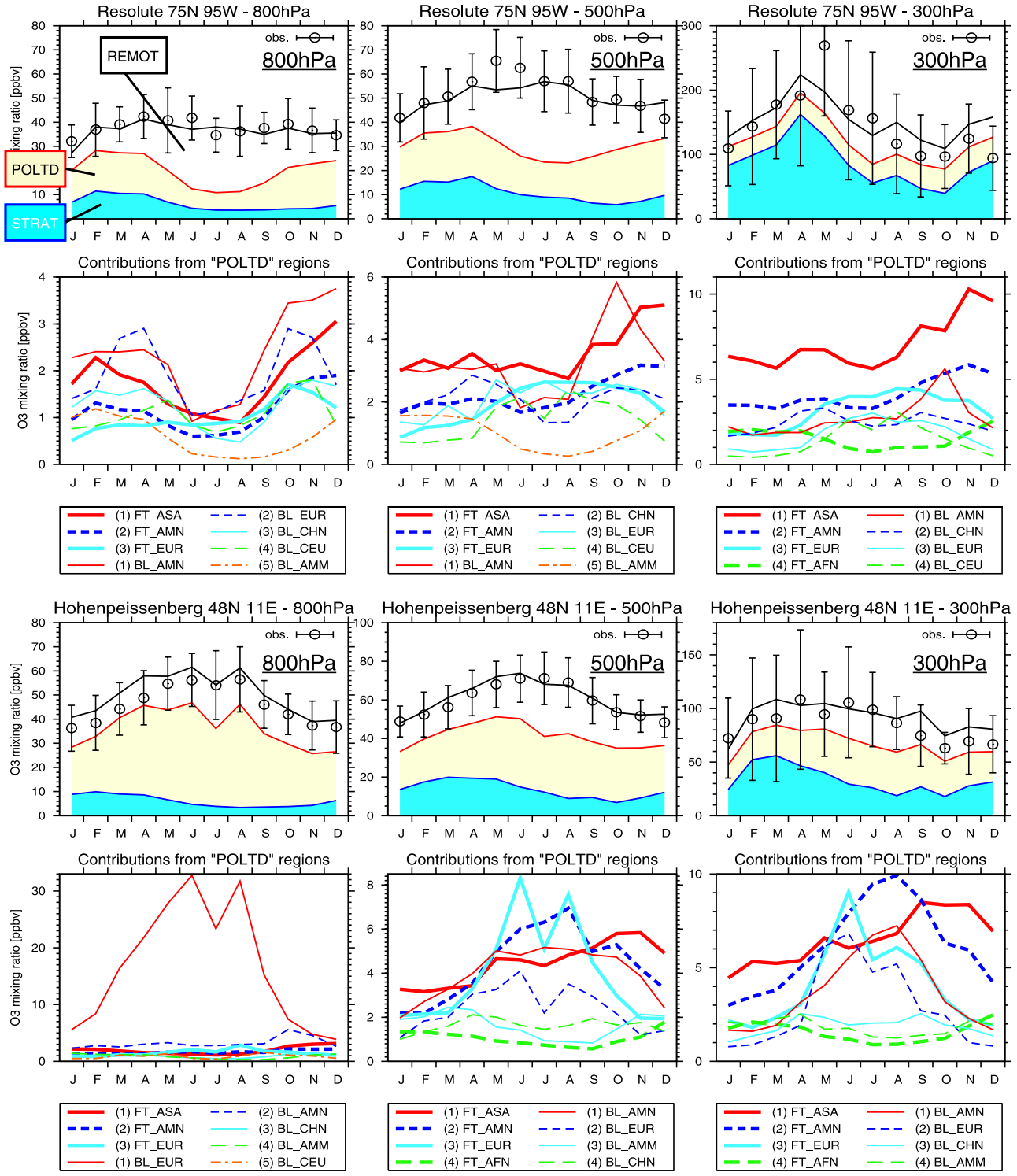

Figure 9. Observed and calculated seasonal variations of O_3 at distinct altitudes with contributions from stratospheric O_3 transport (STRAT), O_3 production in the polluted regions (POLTD), and remote regions (REMOT). In the bottom plot for each site, the top eight contributions of the POLTD regions are shown; key labels are sorted by PBL (BL) and free tropospheric (FT) contributions separately. The observations show climatology taken from *Logan* [1999].

troposphere (FT-ASA) and PBL in the China region (BL-CHN) especially in summer.

[33] An observation study by *Pochanart et al.* [1999] assessed contributions from regional pollution in the China continent to surface O_3 at Oki (36°N, 133°E) located between Sapporo and Kagoshima. We found that the BL-CHN O_3 tracer calculated at Oki well replicates the observation derived Chinese influences at Oki, both showing a

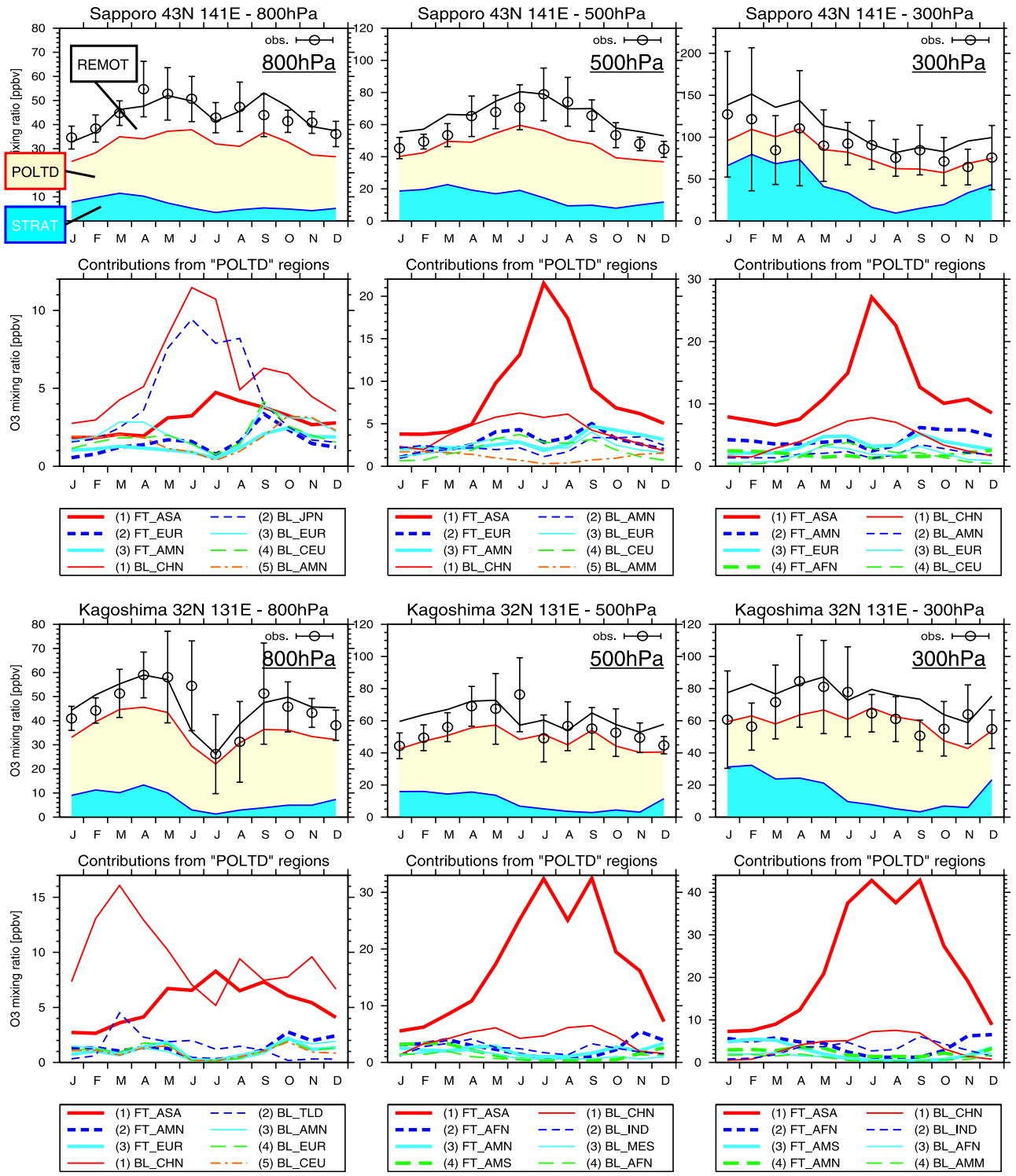

Figure 9. (continued)

significant increase from ~5 ppbv in winter to 20–25 ppbv in summer reflecting intense photochemical O_3 production in the Chinese PBL.

[34] 800 hPa O_3 at Sapporo shows large contributions of 1–3 ppbv from Europe and central Eurasia (EUR and CEU) especially in nonsummer seasons coinciding with transport from North America (AMN) as *Wild et al.* [2004] investigated, which reflect efficient transport over the Eurasian continent toward Asia in winter coupled with the Siberian high-pressure system.

[35] 800 hPa O_3 at Kagoshima (located in a lower latitude than Sapporo), there is a large contribution from Chinese PBL (BL-CHN) with a peak larger than 15 ppbv in March. This BL-CHN O_3 rapidly decreases to ~5 ppbv during April to July unlike Sapporo, but instead O_3 from the Asian free troposphere (FT-ASA) increases because of intense

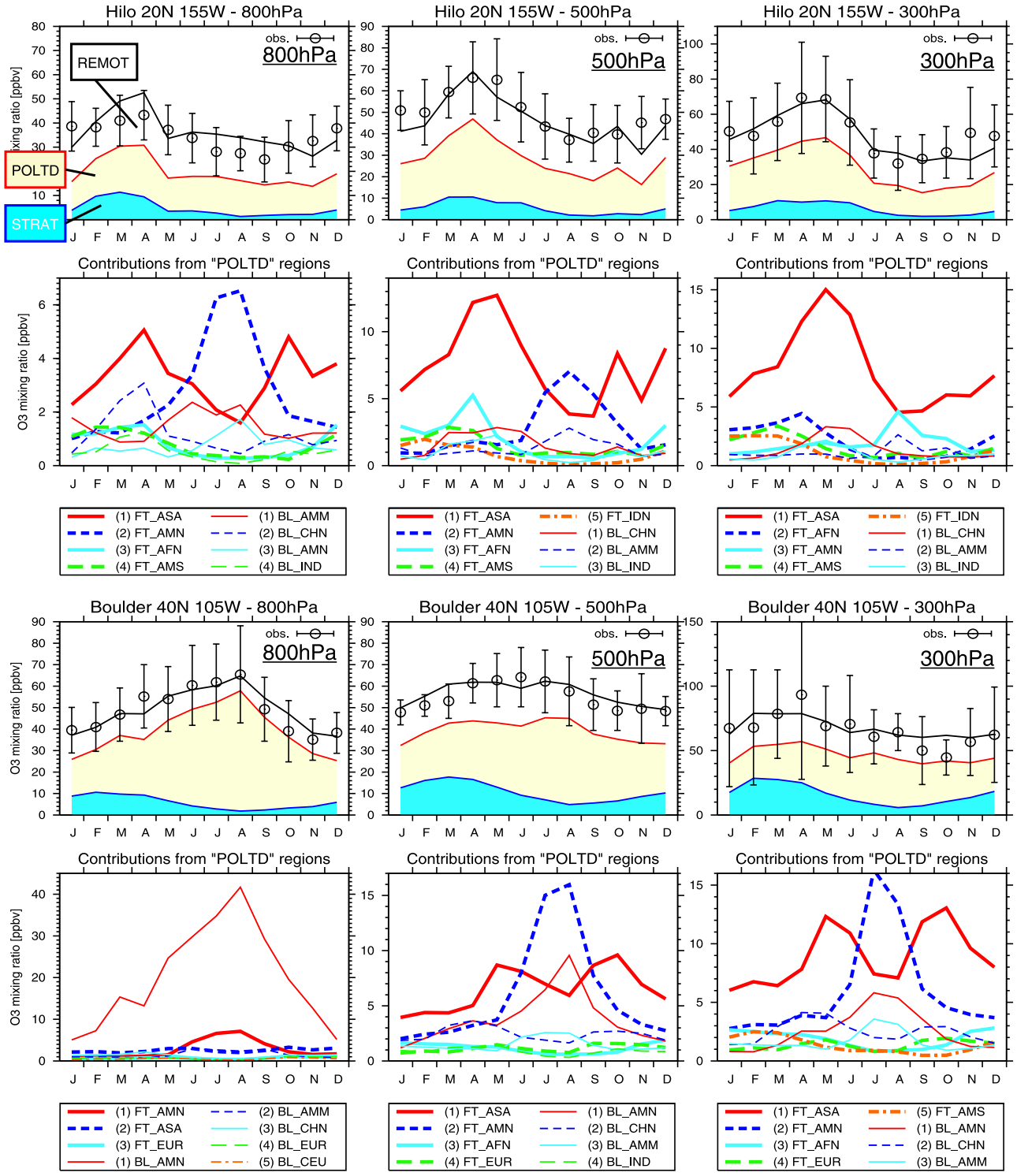

Figure 9. (continued)

chemical O_3 production in summer. It should be also noted that in March there is a large O_3 import (~5 ppbv) from PBL in the Thailand region (BL-TLD) coincident with the BL-CHN O_3 peak, resulting from biomass burning in Southeastern Asia including Thailand as reported by *Tang et al.* [2003]; *Liu et al.* [2003]. At 300 hPa over Kagoshima, the model overestimates the observed total O_3 by ~10 ppbv during June–September. This probably suggests too large contribution from FT-ASA which is most dominant in this season; the O_3 overestimate in winter can be attributed to overestimate of stratospheric O_3 transport.

[36] At Hilo, a remote Pacific site, O_3 seasonality appears to be largely controlled by direct O_3 transport from the polluted regions (POLTD) in spite of long distances there to Hilo. The REMOT O_3 contributions at Hilo are attributable to O_3 production during the long-range transport from the

polluted regions (basically from Asia and North America) over the North Pacific [*Hudman et al.*, 2004]. 800 hPa O_3 displays large contributions from FT-ASA and FT-AMN whose seasonalities appear to be negatively correlated with each other. FT-ASA O_3 decreases toward summer after peaking in April, and in turn O_3 transport from FT-AMN rapidly increases. The summertime large O_3 transport from FT-AMN seen at 800 hPa over Hilo exhibits a ''river of pollution'' [*Staudt et al.*, 2001] flowing in the lower troposphere from the northeastern to the western equatorial Pacific produced by the Pacific High and trade winds. Interestingly, the model shows that O_3 transport from FT-ASA to Hilo follows two different pathways depending on season. While in winter to early spring FT-ASA O_3 is transported directly to Hilo by westerlies, summertime FT-ASA O_3 takes a longer way turning and descending around the Pacific High over the northeastern Pacific and North America and reaches Hilo together with the continental outflow from North America (i.e., FT/BL-AMN O_3). 800 hPa O_3 at Hilo also shows a large contribution from Chinese PBL (BL-CHN) with an April peak coincident with the FT-ASA O_3. At 500 and 300 hPa altitudes, the model shows more dominant contributions from FT-ASA which are most responsible for the spring O_3 maxima at these altitudes. It should be noted that there is a nonnegligible long-range O_3 transport from the North African and South American free troposphere (FT-AFN and FT-AMS) in winter and spring following the eastward pathway toward Asia and the North Pacific as mentioned in the previous section. At Boulder, 800 hPa O_3 seasonal variation largely reflects O_3 production in PBL in the North American region (BL-AMN) showing a strong peak (>40 ppbv) in August. A significant Asian contribution (FT-ASA) is seen through the year ($\sim$3 ppbv) as suggested by *Hudman et al.* [2004]. FT-ASA O_3 increases with altitude to 4–10 ppbv at 500 hPa and 6–14 ppbv at 300 hPa giving significant contribution to O_3 at these altitudes especially in spring and autumn. In summer, North American contributions (FT/BL-AMN) rapidly rise in response to large summertime photochemical O_3 production, but instead the FT-ASA contribution is largely inhibited by less conductive transport over the Pacific in this season. Transport from Chinese PBL (BL-CHN) appears to be a large contributor to 500 and 300 hPa O_3 at Boulder (2–4 ppbv).

3.3. Vertical Profiles

[37] In Figure 10, we examine contributions from the individual source regions to vertical profiles of O_3 over the regions of the NASA aircraft observation campaigns (Global Tropospheric Expeditions) as listed in Table 2. In the Ontario and Atlantic regions (ABLE-3B and SONEX, respectively), the model shows large contributions from O_3 production in North America (FT/BL-AMN) to lower and upper tropospheric O_3. We note that long-range transport from Asian free troposphere gives a primary contribution to the POLTD O_3 calculated in the middle to upper troposphere over these regions. In Hawaii during PEM-West-A, about 50% of O_3 can be explained by transport from the defined source regions (POLTD). In the upper troposphere, the model shows an outstanding contribution (>10 ppbv) from Asian free troposphere (FT-ASA) followed by significant O_3 transport from Chinese PBL (BL-CHN) and North American free troposphere (FT-AMN). Contribution from Asian free troposphere is ranked first also in the upper troposphere over the Philippine Sea region (during PEM-West-B), Japan and China-Coast regions (TRACE-P) where O_3 vertical profiles are largely controlled by transport from the source regions (POLTD). BL-CHN O_3, giving significant contribution to the lower troposphere over the Japan and China-Coast regions, is estimated to be equivalent to BL-JPN O_3 at the surface of the Japan region. In the lower troposphere over the China-Coast region, there is significant O_3 import reaching 5 ppbv from the Thailand PBL region (BL-TLD) coinciding with biomass burning in Southeastern Asia [*Tang et al.*, 2003; *Liu et al.*, 2003] as also seen in 800 hPa O_3 at Kagoshima in Figure 9; tagged CO simulation in this study similarly shows significant CO transport from Thailand and Indian regions ($\sim$30 ppbv, individually) at 1–3 km altitude over this region (not shown). It should be noted that the model reveals significant long-range O_3 exports from North African and South American free troposphere (FT-AFN and FT-AMS) which increase individually upper tropospheric O_3 over the Japan and China Coast regions by 3–7 ppbv. The export pathway from FT-AFN and FT-AMS to these regions are already described with respect to Figure 7 in the previous section. In the remote Pacific regions during PEM-Tropics-A and B, 30–70% of TROPO O_3 (tropospheric origin) can be explained by transport from the POLTD source regions. The POLTD O_3 in these regions is composed in general of contributions from North, central, and South America (AMN, AMM, and AMS), North and South Africa (AFN and AFS), Indonesia (IDN), and Asia (ASA). It is remarkable that Asian free tropospheric O_3 (FT-ASA) gives the largest contributions in the middle-upper troposphere in the southern tropical regions: Tahiti, Fiji, and Easter Island during PEM-Tropics-A. This significant contribution from Asia is a result of long-range interhemispheric O_3 transport from Asian free troposphere to the southern midlatitudes via the western Indian Ocean, Africa, and the Atlantic, which is described already (Figure 7). In Tahiti during PEM-Tropics-B, the largest O_3 contribution is from South America (FT-AMS) in the lower troposphere, but from Australia (FT-AUS) in the upper troposphere. Similar vertical structure is also seen in our tagged CO tracers over Tahiti (not shown), and is linked to the Walker circulation in the tropics: i.e., westward transport from South America to Tahiti in the lower troposphere over the eastern Pacific, and eastward transport from Australia in the upper troposphere over the western Pacific.

[38] In the biomass burning related regions during TRACE-A expedition, the model shows large contributions of the POLTD source regions coming mostly from O_3 production in PBL and free troposphere in South America and North/South Africa as suggested by *Thompson et al.* [1996], *Thompson and Hudson* [1999], and *Jenkins et al.* [2003]. In 5–10 km altitudes over the eastern Brazil region (E-Brazil) there is enhanced O_3 coming from South American PBL (BL-AMS) which gives an important contribution to upper tropospheric O_3 levels in this region. This appears to be associated with convective uplifting of the PBL air to the upper troposphere in the eastern Brazilian region as revealed by *Fishman et al.* [1996]. It should be noted that there are O_3 exports of a few ppbv from Asian free troposphere in each of the TRACE-A regions since these

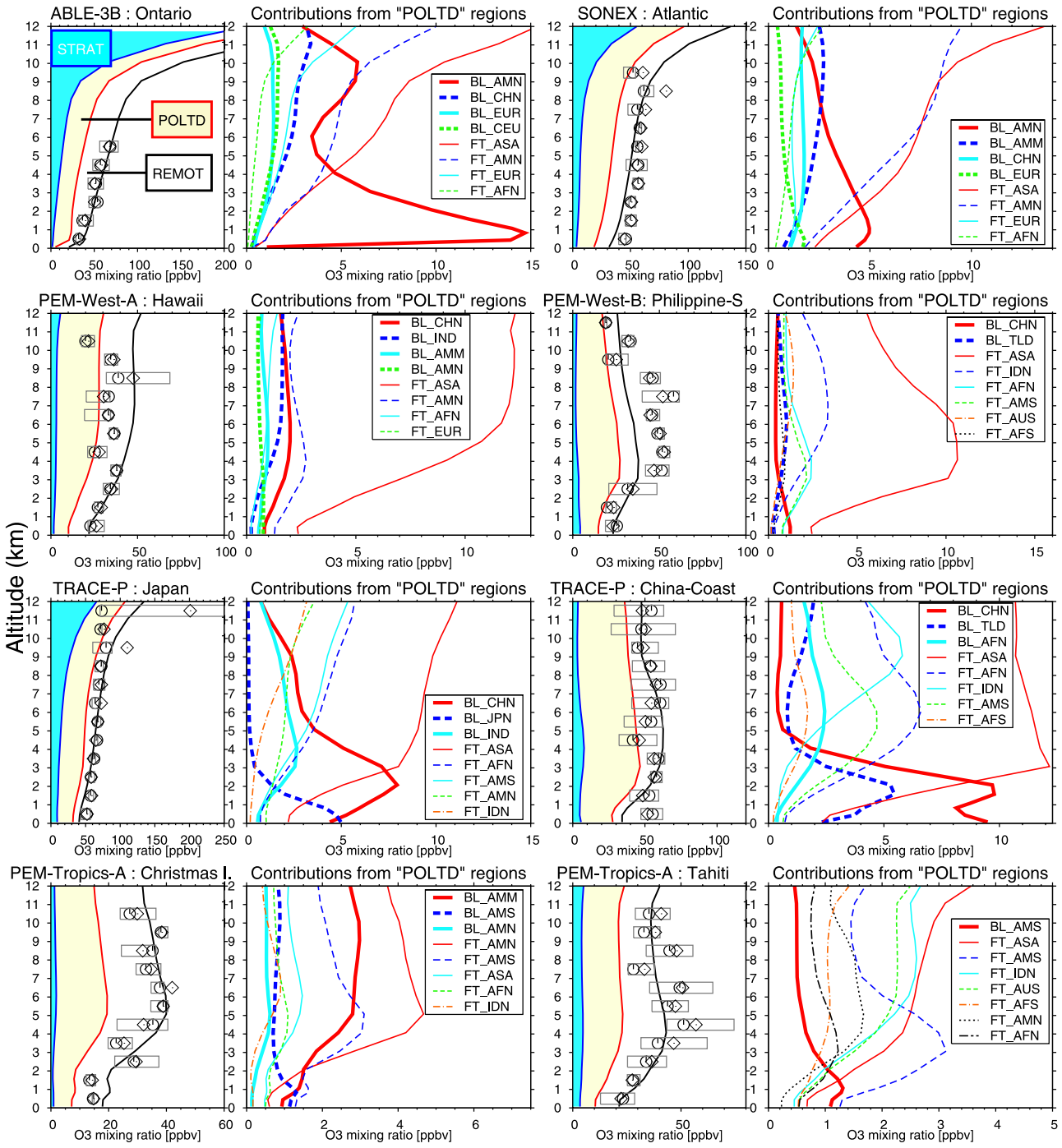

Figure 10. O_3 vertical profiles observed and calculated over the regions of GTE campaigns (listed in Table 2) with contributions from stratospheric O_3 transport (STRAT), O_3 production in the polluted regions (POLTD), and remote regions (REMOT). In the right plot for each region, the top eight contributions of the POLTD regions are shown; key labels are sorted by PBL (BL) and free tropospheric (FT) contributions separately (see Table 1 for region definition). The observations show mean (diamonds), median (circles), and inner 50% of the data (boxes) for the NASA GTE campaigns.

regions are on the pathway of interhemispheric transport from Asia to the southern midlatitudes as discussed above.

3.4. Global Budgets

[39] In Table 3, we summarize detailed global budgets of O_3 from various source regions: stratosphere STRAT, remote troposphere REMOT, and polluted source regions POLTD. 63% of the calculated chemical O_3 production in the global troposphere (4723 TgO_3/yr) comes from the POLTD regions, of which South American and Asian free troposphere (FT-AMS and FT-ASA) shows particularly large O_3 production (295 and 325 TgO_3/yr, respectively).

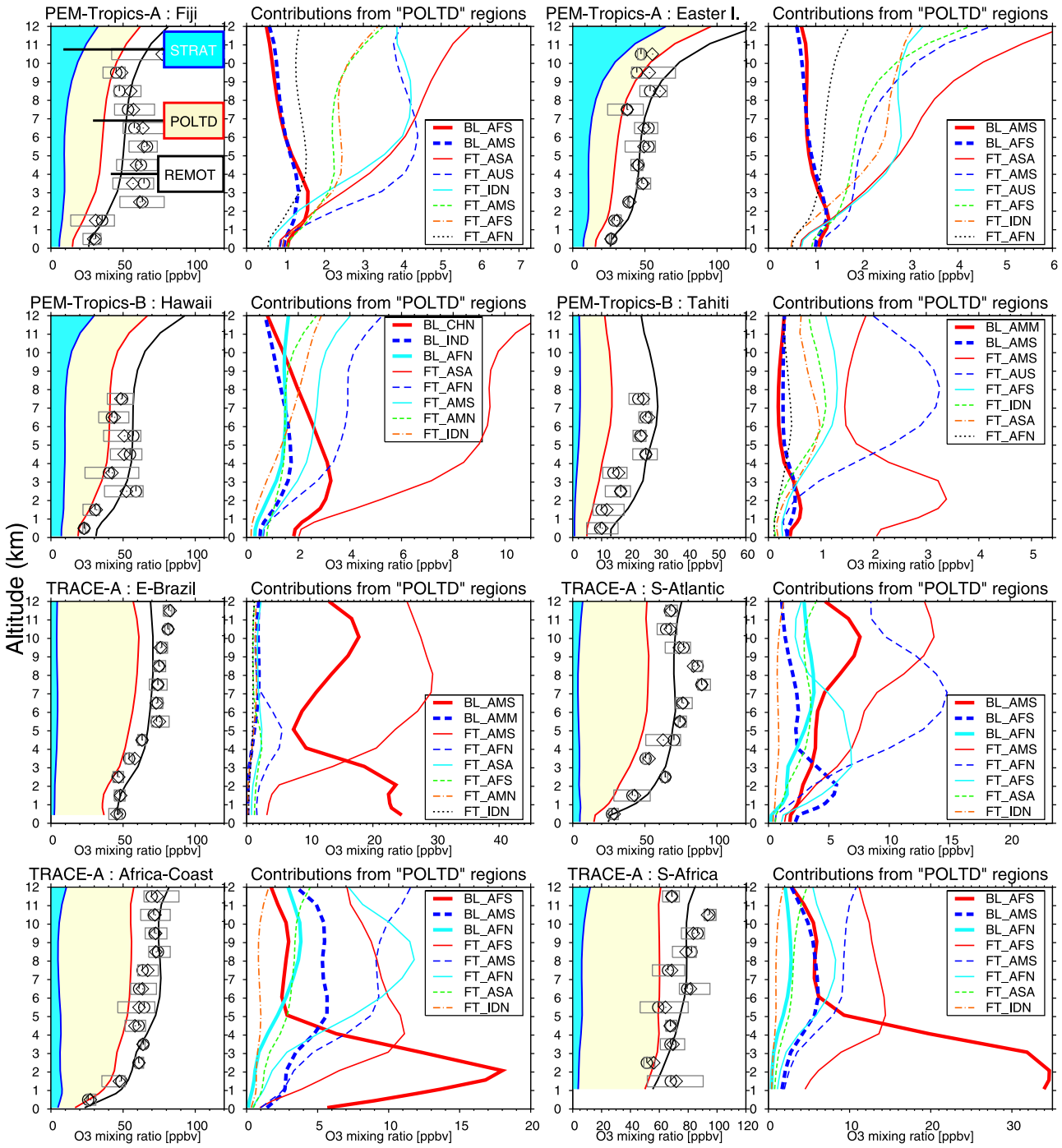

Figure 10. (continued)

[40] Concerning O_3 input/output associated with stratosphere-troposphere exchange, the model estimates the net input of stratospheric O_3 (STRAT) as 616 TgO_3/yr and output of tropospheric origin O_3 (TROPO = REMOT + POLTD) as 121 TgO_3/yr, leading to a net O_3 influx from the stratosphere to troposphere of 494 TgO_3/yr. Significant transport to the stratosphere is calculated with O_3 produced in the FT-AMN, FT-AMS, and FT-ASA regions (6.6, 5.8, and 8.0 TgO_3/yr, respectively). Although transport of the PBL O_3 tracers to the stratosphere is much smaller than those of the free tropospheric tracers (FT tracers), relatively large output to the stratosphere (~1 TgO_3/yr) is seen for O_3 from North American, Indian, and Chinese PBL (BL-AMN, IND, and CHN).

[41] The model calculates an annual mean global tropospheric O_3 burden of 344 Tg: of which 23% from the stratosphere (STRAT), 29% from the remote troposphere (REMOT), and 48% from the polluted source regions (POLTD). The most significant contributor of the POLTD tracers is Asian free troposphere (FT-ASA, 25 Tg) followed by South American free troposphere (FT-AMS, 21 Tg). It should be noted also that O_3 exported from FT-ASA is

Table 3. Global Budget of Tropospheric O_3 From Distinct Source Regions

					Tropospheric Burden, TgO_3		Lifetime, days	
Tracer ID[a]	P[b]	P-L[c]	Deposition	STE[d]	Global, %	NH	Chemical	Total[e]
O_3-ALL	4723	422.5	−917	494.2	343.5 (100.0%)	186.3	26	22
STRAT	0	−484.1	−131	615.6	77.9 (22.7%)	38.6	45	37
REMOT	1735	338.7	−257	−81.7	101.0 (29.4%)	51.1	25	21
POLTD	2988	567.9	−528	−39.7	164.6 (47.9%)	96.5	23	20
BL-AMN	154	48.0	−47	−0.7	6.7 (1.9%)	6.5	24	16
BL-AMM	162	29.8	−30	−0.3	6.6 (1.9%)	5.5	18	15
BL-AMS	203	49.6	−49	−0.3	7.4 (2.2%)	0.9	18	13
BL-AFN	166	33.1	−33	−0.2	5.4 (1.6%)	4.0	15	12
BL-AFS	175	38.8	−38	−0.3	6.6 (1.9%)	0.9	17	14
BL-EUR	111	44.1	−44	−0.3	4.3 (1.3%)	4.2	27	14
BL-CEU	72	27.8	−28	−0.3	2.8 (0.8%)	2.8	28	14
BL-MES	92	22.3	−22	0.0	3.2 (0.9%)	2.9	17	13
BL-IND	97	20.9	−20	−0.8	3.9 (1.1%)	3.4	18	14
BL-TLD	50	7.8	−7	−0.4	2.2 (0.6%)	1.7	18	16
BL-CHN	128	34.6	−34	−1.0	5.9 (1.7%)	5.5	23	17
BL-JPN	22	6.4	−6	0.0	1.1 (0.3%)	1.1	24	18
BL-IDN	61	9.7	−9	−0.5	2.8 (0.8%)	0.9	19	17
BL-AUS	88	19.7	−19	−0.3	3.7 (1.1%)	0.2	20	15
FT-AMN	163	25.6	−19	−6.6	11.6 (3.4%)	10.5	29	26
FT-AMS	295	32.9	−27	−5.8	21.0 (6.1%)	7.0	27	26
FT-AFN	203	21.2	−19	−2.2	13.4 (3.9%)	9.1	25	24
FT-AFS	186	21.6	−18	−3.8	13.1 (3.8%)	2.1	27	25
FT-EUR	58	14.5	−12	−2.6	4.1 (1.2%)	4.0	34	25
FT-ASA	325	39.7	−32	−8.0	24.9 (7.2%)	20.5	30	28
FT-IDN	90	8.9	−7	−2.2	6.9 (2.0%)	2.2	29	28
FT-AUS	86	11.0	−8	−3.2	6.9 (2.0%)	0.8	31	29

[a]For definition, see Table 1 and Figure 2.
[b]Gross chemical production in the troposphere(TgO_3/yr).
[c]Net chemical production in the troposphere(TgO_3/yr).
[d]Stratosphere-troposphere exchange (TgO_3/yr): net O_3 flux from the stratosphere (negative values represent export to the stratosphere).
[e]Residence time in the troposphere.

relatively abundant even in the SH (4.4 Tg), and likewise FT-AMS O_3 is abundant even in the NH (7 Tg), resulting from the long-range interhemispheric transport from these regions as described above.

[42] In this simulation, the chemical and total (residential) lifetimes of global tropospheric O_3 are estimated to be 26 and 22 days, respectively. O_3 from the stratosphere (STRAT) shows longer lifetimes than tropospheric origin O_3 (REMOT and POLTD) because of slower chemical O_3 destruction and absence of dry deposition in the upper troposphere where most of STRAT O_3 is distributed. Similarly, the lifetimes estimated for free tropospheric O_3 (FT tracers) are generally larger than those for PBL O_3 (BL tracers), causing a larger global burden of FT O_3 relative to BL O_3. Total lifetime for the BL tracers is significantly smaller than chemical lifetime for them since large part of PBL O_3 is subject to dry deposition at the surface as well as chemical destruction. In particular, total lifetime for O_3 tracers from European and central Eurasian PBL regions (BL-EUR and BL-CEU) is two times smaller than chemical one for them reflecting large dry deposition as they crawl over the Eurasian Continent toward Asia and the Pacific (see discussion in section 3.2).

4. Summary and Conclusions

[43] We investigated detailed source attribution of global distribution and budget of tropospheric O_3 using a tagged tracer simulation. This study focused mainly on transport from source regions over the globe with using O_3 tracers tagged by the individual source regions, and demonstrated how regional to interhemispheric transport control the global distribution and seasonal cycle of tropospheric O_3. For tagging O_3, we considered chemical production in various source regions in the PBL and free troposphere; the model separately transports 14 and 7 O_3 tracers tagged by chemical production in the PBL and free troposphere, respectively, in addition to a stratospheric O_3 tracer.

[44] In the low to midlatitudes, O_3 transport from the polluted source regions like North/South America, Europe, and Asia generally accounts for more than 50% of ozone even in remote locations. In the northern high latitudes, contributions of O_3 transport from polluted source regions, remote troposphere, and stratosphere were estimated to be comparable with each other ($\sim$10 DU in annual mean). We found that in particular O_3 exported from the free troposphere in North/South America, Africa, and Asia distributes extensively over the globe with a peak of 5–12 DU in annual mean.

[45] Near the surface, our simulation showed, there are extensive O_3 outflows from the PBL regions in North America, Europe, central Eurasia, and China in the NH with downward O_3 transport from the free troposphere (especially in North America and Asia). In the upper troposphere, we found large O_3 contributions from the free troposphere in North/South America, Africa, and Asia extending on a hemispheric to global scale, which are resulting from intense injection of precursors from the surface associated with anthropogenic emissions including biomass burning, and also from lightning NO_x production

over the regions. O_3 originating from the Asian free troposphere was simulated to cause particularly large contributions to the upper tropospheric O_3 abundances in the NH with the range of 5–30 ppbv in annual mean. We found that this O_3 outflow from the Asian free troposphere plays a key role in seasonal variation and vertical profile of O_3 in the global troposphere. We also identified an interhemispheric transport pathway in the upper troposphere that conveys O_3 produced in the Asian free troposphere to the SH midlatitudes via the western Indian Ocean, Africa, and Atlantic causing a 5–10 ppbv O_3 contribution to the upper troposphere in the South Pacific in June–September. Our simulation demonstrated that there is a significant interhemispheric O_3 transport from South America to the NH midlatitudes in the upper troposphere which reach Japan, North Pacific, and U.S. in conjunction with O_3 export from North Africa; in the upper troposphere over Japan in spring, the model calculated significant O_3 contributions of ~5 ppbv from South America and North Africa (amounting to ~10 ppbv).

[46] In this study, annual mean global tropospheric O_3 burden was calculated to be 344 Tg as the sum of chemical production in the polluted source regions 165 Tg (48%) and in the remote regions 101 Tg (29%), and stratosphere-troposphere exchange 78 Tg (23%). We found a particularly large O_3 burden for chemical production in the free troposphere in Asia and South America (25 and 21 Tg, respectively).

[47] As shown above, this study attributed the global distribution of tropospheric O_3 to various source origins and regions, and revealed the mechanism of regional to interhemispheric transport. Long-range O_3 transport over the major pathways in the NH (such as the trans-Pacific and Eurasia) simulated in this study appears consistent with the previous studies which investigated long-range impacts of anthropogenic emissions on O_3 in downwind locations [e.g., *Holloway et al.*, 2003; *Wild et al.*, 2004]. It should be, however, noted that our tagged O_3 tracer does not differentiate between anthropogenic origin and natural one as from lightning NO_x emissions. To more quantitatively identify long-range transport of anthropogenic O_3, we need to introduce an emission sensitivity study to our tagged tracer approach as a future work. This kind of study can be also applied to investigation of impacts of future emission changes as expected in Asia on the global air quality.

[48] **Acknowledgments.** This research has been partially supported by Global Environmental Research Fund (B051), Japan Ministry of Environment. In this study, we used the Earth Simulator of the Japan Agency for Marine-Earth Science and Technology (JAMSTEC) in cooperation with Project for Sustainable Coexistence of Human, Nature, and the Earth (Japan Ministry of Education, Culture, Sports, Science and Technology).

References

Akimoto, H. (2003), Global air quality and pollution, *Science*, *302*(5651), 1609–1844.

Arino, O., J.-M. Rosaz, and J.-M. Melinotte (1999), World Fire Atlas with AVHRR and ATSR, paper presented at IUFRO Conference on Remote Sensing and Forest Monitoring, Int. Union of For. Res. Organ., Rogow, Poland.

Auvray, M., and I. Bey (2005), Long-range transport to Europe: Seasonal variations and implications for the European ozone budget, *J. Geophys. Res.*, *110*, D11303, doi:10.1029/2004JD005503.

Barry, R., and R. Chorley (2003), *Atmosphere, Weather and Climate*, 8th ed., 421 pp., Routledge, Boca Raton, Fla.

Berntsen, T. K., I. S. A. Isaksen, G. Myhre, J. S. Fuglestvedt, F. Stordal, T. A. Larsen, R. S. Freckleton, and K. P. Shine (1997), Effects of anthropogenic emissions on tropospheric ozone and its radiative forcing, *J. Geophys. Res.*, *102*(D23), 28,101–28,126.

Berntsen, T. K., S. Karlsdóttir, and D. Jaffe (1999), Influence of Asian emissions on the composition of air reaching the North Western United States, *Geophys. Res. Lett.*, *26*, 2171–2174.

Bey, I., D. Jacob, J. Logan, and R. Yantosca (2001), Asian chemical outflow to the Pacific: Origins, pathways and budgets, *J. Geophys. Res.*, *106*, 23,097–23,113.

Browning, K. A., and N. M. Roberts (1994), Structure of a frontal cyclone, *Q. J. R. Meteorol. Soc.*, *122*, 1845–1872.

Chatfield, R. B., Z. Guo, G. W. Sachse, D. R. Blake, and N. J. Blake (2002), The subtropical global plume in the Pacific Exploratory Mission-Tropics A (PEM-Tropics A), PEM-Tropics B, and the Global Atmospheric Sampling Program (GASP): How tropical emissions affect the remote Pacific, *J. Geophys. Res.*, *107*(D16), 4278, doi:10.1029/2001JD000497.

Cooper, O. R., et al. (2006), Large upper tropospheric ozone enhancements above midlatitude North America during summer: In situ evidence from the IONS and MOZAIC ozone measurement network, *J. Geophys. Res.*, *111*, D24S05, doi:10.1029/2006JD007306.

Derwent, R. G., D. S. Stevenson, W. J. Collins, and C. E. Johnson (2004), Intercontinental transport and the origins of the ozone observed at surface sites in Europe, *Atmos. Environ.*, *38*, 1891–1901.

Edwards, D. P., et al. (2003), Tropospheric ozone over the tropical Atlantic: A satellite perspective, *J. Geophys. Res.*, *108*(D8), 4237, doi:10.1029/2002JD002927.

Emori, S., T. Nozawa, A. Numaguti, and I. Uno (2001), Importance of cumulus parameterization for precipitation simulation over east Asia in June, *J. Meteorol. Soc. Jpn.*, *79*, 939–947.

Fan, S.-M., D. J. Jacob, D. L. Mauzerall, J. D. Bradshaw, S. T. Sandholm, D. R. Blake, R. W. T. H. B. Singh, G. L. Gregory, and G. W. Sachse (1994), Photochemistry of reactive nitrogen in the sub Arctic troposphere in summer 1990: Observation and modeling, *J. Geophys. Res.*, *99*, 16,867–16,878.

Fischer, H., et al. (2002), Deep convective injection of boundary layer air into the lowermost stratosphere at midlatitudes, *Atmos. Chem. Phys. Disc.*, *2*, 2003–2019.

Fishman, J., et al. (1996), The NASA GTE TRACE A Experiment (September–October 1992): Overview, *J. Geophys. Res.*, *101*, 23,865–23,879.

Fishman, J., A. Wozniak, and J. Creilson (2003), Global distribution of tropospheric ozone from satellite measurements using the empirically corrected tropospheric ozone residual technique: Identification of the regional aspects of air pollution, *Atmos. Chem. Phys.*, *3*, 893–907.

Follows, M., and J. Austin (1992), A zonal average model of the stratospheric contributions to the tropospheric ozone budget, *J. Geophys. Res.*, *97*, 18,047–18,060.

Forster, P. M., C. E. Johnson, K. S. Law, J. A. Pyle, and K. P. Shine (1996), Further estiates of radiative forcing due to tropospheric ozone changes, *Geophys. Res. Lett.*, *23*, 3321–3324.

Gauss, M., et al. (2003), Radiative forcing in the 21st century due to ozone changes in the troposphere and the lower stratosphere, *J. Geophys. Res.*, *108*(D9), 4292, doi:10.1029/2002JD002624.

Gauss, M., et al. (2006), Radiative forcing since preindustrial times due to ozone change in the troposphere and the lower stratosphere, *Atmos. Chem. Phys.*, *6*, 575–599.

Hannan, J. R., H. E. Fuelberg, J. H. Crawford, G. W. Sachse, and D. R. Blake (2003), Role of wave cyclones in transporting boundary layer air to the free troposphere during the spring 2001 NASA/TRACE-P experiments, *J. Geophys. Res.*, *108*(D20), 8785, doi:10.1029/2002JD003105.

Holloway, T., A. Fiore, and M. G. Hastings (2003), Intercontinental transport of air pollution: Will emerging science lead to a new hemispheric treaty?, *Environ. Sci. Technol.*, *37*(20), 4535–4542, doi:10.1021/es034031g.

Horowitz, L. W., et al. (2003), A global simulation of tropospheric ozone and related tracers: Description and evaluation of MOZART, version 2, *J. Geophys. Res.*, *108*(D24), 4784, doi:10.1029/2002JD002853.

Hudman, R. C., et al. (2004), Ozone production in transpacific Asian pollution plumes and implications for ozone air quality in California, *J. Geophys. Res.*, *109*, D23S10, doi:10.1029/2004JD004974.

Jacob, D. J., J. A. Logan, and P. P. Murti (1999), Effect of rising Asian emissions on surface ozone in the United States, *Geophys. Res. Lett.*, *26*, 2175–2178.

Jacob, D. J., et al. (2003), Transport and Chemical Evolution over the Pacific (TRACE-P) aircraft mission: Design, execution, and first results, *J. Geophys. Res.*, *108*(D20), 9000, doi:10.1029/2002JD003276.

Jenkins, G. S., J.-H. Ryu, A. M. Thompson, and J. C. Witte (2003), Linking horizontal vertical transports of biomass fire emissions to the Tropical Atlantic Ozone Paradox during the Northern Hemisphere winter season:

1999, *J. Geophys. Res.*, *108*(D23), 4745, doi:10.1029/2002JD003297.
Junge, C. E. (1962), Global ozone budget and exchange between stratosphere troposphere, *Tellus*, *14*, 363–377.
Lawrence, M. G., R. von Kuhlmann, and M. Salzmann (2003a), The balance of effects of deep convective mixing on tropospheric ozone, *Geophys. Res. Lett.*, *30*(18), 1940, doi:10.1029/2003GL017644.
Lawrence, M. G., et al. (2003b), Global chemical weater forecasts for field campaign planning: Predictions and observations of large-scale features during MINOS, CONTRACE, and INDOEX, *Atmos. Chem. Phys.*, *3*, 267–289.
Li, Q., et al. (2001), A tropospheric ozone maximum over the Middle East, *Geophys. Res. Lett.*, *28*(17), 3235–3238.
Li, Q., D. J. Jacob, T. Fairlie, H. Liu, R. Martin, and R. Yantosca (2002a), Stratospheric versus pollution influences on ozone at Bermuda: Reconciling past analyses, *J. Geophys. Res.*, *107*(22), 4611, doi:10.1029/2002JD002138.
Li, Q., et al. (2002b), Transatlantic transport of pollution and its effects on surface ozone in Europe and North America, *J. Geophys. Res.*, *107*(13), 4166, doi:10.1029/2001JD001422.
Lin, S.-J., and R. B. Rood (1996), Multidimensional flux-form semi-Lagrangian transport schemes, *Mon. Weather Rev.*, *124*, 2046–2070.
Liu, H., D. J. Jacob, L. Y. Chan, S. J. Oltmans, I. Bey, R. M. Yantosca, J. M. Harris, B. N. Duncan, and R. V. Martin (2002), Sources of tropospheric ozone along the Asian Pacific Rim: An analysis of ozonesonde observations, *J. Geophys. Res.*, *107*(D21), 4573, doi:10.1029/2001JD002005.
Liu, H., D. J. Jacob, I. Bey, R. M. Yantosca, and B. N. Duncan (2003), Transport pathway for Asian pollution outflow over the Pacific: Interannual and seasonal variations, *J. Geophys. Res.*, *108*(D20), 8786, doi:10.1029/2002JD003102.
Logan, J. A. (1999), An analysis of ozonesonde data for the troposphere: Recommendations for testing 3-D models and development of a gridded climatology for tropospheric ozone, *J. Geophys. Res.*, *104*, 16,115–16,149.
Ma, J., H. Liu, and D. Hauglustaine (2002), Summertime tropospheric ozone over China simulated with a regional chemical transport model: 1. Model description and evaluation, *J. Geophys. Res.*, *107*(D22), 4660, doi:10.1029/2001JD001354.
Mickley, L. J., P. P. Murti, D. J. Jacob, J. A. Logan, D. M. Koch, and D. Rind (1999), Radiative forcing from tropospheric ozone calculated with a unified chemistry-climate model, *J. Geophys. Res.*, *104*, 30,153–30,172.
Mickley, L. J., D. J. Jacob, and D. Rind (2004), Climate response to the increase in tropospheric ozone since preindustrial times: A comparison between ozone and equivalent CO_2 forcings, *J. Geophys. Res.*, *109*, D05106, doi:10.1029/2003JD003653.
Moxim, W. J., H. Levy II, and P. S. Kashibhatla (1996), Simulated global tropospheric PAN: Its transport and impact on NO_x, *J. Geophys. Res.*, *101*, 12,621–12,638.
Nagashima, T., H. Shiogama, T. Yokohata, T. Takemura, S. A. Crooks, and T. Nozawa (2006), Effects of carbonaceous aerosols on surface temperature in the mid twentieth century, *Geophys. Res. Lett.*, *33*, L04702, doi:10.1029/2005GL024887.
Nozawa, T., T. Nagashima, H. Shiogama, and S. A. Crooks (2005), Detecting natural influence on surface air temperature change in the early twentieth century, *Geophys. Res. Lett.*, *32*, L20719, doi:10.1029/2005GL023540.
Numaguti, A. (1993), Dynamics and energy balance of the Hadley circulation and the tropical precipitation zones: Significance of the distribution of evaporation, *J. Atmos. Sci.*, *50*, 1874–1887.
Numaguti, A., M. Takahashi, T. Nakajima, and A. Sumi (1995), Development of an atmospheric general circulation model, in *Reports of a New Program for Creative Basic Research Studies, Studies of Global Environment Change With Special Reference to Asia and Pacific Regions*, *Rep. I–3*, pp. 1–27, Cent. for Clim. Syst. Res., Tokyo.
Olivier, J. G. J. et al. (1996), Description of EDGAR Version 2.0. A set of global emission inventories of greenhouse gases and ozone-depleting substances for all anthropogenic and most natural sources on a per country basis and on $1° \times 1°$ grid, *RIVM Rep. 771060 002/TNO*, Natl. Inst. for Public Health and the Environ., Bilthoven, Netherlands.
Piketh, S. J., R. J. Swap, W. Maenhaut, H. J. Annegarn, and P. Formenti (2002), Chemical evidence of long-range atmospheric transport over southern Africa, *J. Geophys. Res.*, *107*(D24), 4817, doi:10.1029/2002JD002056.
Pochanart, P., J. Hirokawa, Y. Kajii, and H. Akimoto (1999), Influence of regional-scale anthropogenic activity in northeast Asia on seasonal variations of surface ozone and carbon monoxide observed at Oki, Japan, *J. Geophys. Res.*, *104*, 3621–3631.
Price, C., and D. Rind (1994), Possible implications of global climate change on global lightning distributions and frequencies, *J. Geophys. Res.*, *99*, 10,823–10,831.
Roelofs, G.-J., and J. Lelieveld (1997), Model study of the influcence of cross-tropopause O_3 transport on tropospheric O_3 levels, *Tellus, Ser. B*, *49*, 38–55.
Russel, J. M., III, et al. (1993), The halogen occultation experiment, *J. Geophys. Res.*, *98*, 10,777–10,798.
Staudt, A., D. Jacob, J. Logan, D. Bachiochi, T. Krishnamurti, and G. Sachse (2001), Continental sources, transoceanic transport, and interhemispheric exchange of carbon monoxide over the Pacific, *J. Geophys. Res.*, *106*, 32,571–32,589.
Stohl, A., S. Eckhardt, C. Forster, P. James, and N. Spichtinger (2002), On the pathways and timescales of intercontinental air pollution transport, *J. Geophys. Res.*, *107*(D23), 4684, doi:10.1029/2001JD001396.
Sudo, K., M. Takahashi, J. Kurokawa, and H. Akimoto (2002a), CHASER: A global chemical model of the troposphere: 1. Model description, *J. Geophys. Res.*, *107*(D17), 4339, doi:10.1029/2001JD001113.
Sudo, K., M. Takahashi, and H. Akimoto (2002b), CHASER: A global chemical model of the troposphere: 2. Model results and evaluation, *J. Geophys. Res.*, *107*(D21), 4586, doi:10.1029/2001JD001114.
Takigawa, M., M. Takahashi, and H. Akiyoshi (1999), Simulation of ozone and other chemical species using a Center for Climate System Research/National Institute for Environmental Studies atmospheric GCM with coupled stratospheric chemistry, *J. Geophys. Res.*, *104*, 14,003–14,018.
Tang, Y., et al. (2003), Influences of biomass burning during the Transport and Chemical Evolution Over the Pacific (TRACE-P) experiment identified by the regional chemical transport model, *J. Geophys. Res.*, *108*(D21), 8824, doi:10.1029/2002JD003110.
Thompson, A. M., and R. D. Hudson (1999), Tropical tropospheric ozone (TTO) maps from Nimbus 7 and Earth Probe TOMS by the modified-residual method: Evaluation with sondes, ENSO signals, and trends from Atlantic regional time series, *J. Geophys. Res.*, *104*, 26,961–26,975.
Thompson, A. M., K. E. Pickering, D. P. McNamara, M. R. Schoeberl, R. D. Hudson, J. H. Kim, E. V. Browell, V. W. J. H. Kirchhoff, and D. Nganga (1996), Where did tropospheric ozone over southern Africa and the tropical Atlantic come from in October 1992? Insights from TOMS, GTE/TRACE-A and SAFARI-92, *J. Geophys. Res.*, *101*, 24,251–24,278.
Thompson, A. M., et al. (2000), A tropical Atlantic paradox: Shipboard and satellite views of a tropospheric ozone maximum and wave-one in January–February 999, *Geophys. Res. Lett.*, *27*, 3317–3320.
Thompson, A. M., J. C. Witte, R. D. Hudson, H. Guo, J. R. Herman, and M. Fujiwara (2001), Tropical tropospheric ozone and biomass burning, *Science*, *291*, 2128–2132.
van Leer, B. (1977), Toward the ultimate conservative difference scheme. Part IV: A new approach to numerical convection, *J. Comput. Phys.*, *23*, 276–299.
van Noije, T. P. C., et al. (2006), Multi-model ensemble simulations of tropospheric NO_2 compared with GOME retrievals for the year 2000, *Atmos. Chem. Phys.*, *6*, 2943–2979.
von Kuhlmann, R., M. Lawrence, and P. Crutzen (2003), A model for studies of tropospheric ozone and nonmethane hydrocarbons: Model description and ozone results, *J. Geophys. Res.*, *108*(D9), 4294, doi:10.1029/2002JD002893.
Wang, Y., D. J. Jacob, and J. A. Logan (1998a), Global simulation of tropospheric O_3-NO_x-hydrocarbon chemistry: 1. Model formulation, *J. Geophys. Res.*, *103*, 10,713–10,725.
Wang, Y., J. A. Logan, and D. J. Jacob (1998b), Global simulation of tropospheric O_3-NO_x-hydrocarbon chemistry: 2. Model evaluation and global ozone budget, *J. Geophys. Res.*, *103*, 10,727–10,755.
Wang, Y., D. J. Jacob, and J. A. Logan (1998c), Global simulation of tropospheric O_3-NO_x-hydrocarbon chemistry: 3. Origin of tropospheric ozone and effects of nonmethane hydrocarbons, *J. Geophys. Res.*, *103*, 10,757–10,767.
Wild, O., and H. Akimoto (2001), Intercontinental transport of ozone and its precursors in a three-dimensional global CTM, *J. Geophys. Res.*, *106*, 27,729–27,744.
Wild, O., P. Pochanart, and H. Akimoto (2004), Trans-Eurasian transport of ozone and its precursors, *J. Geophys. Res.*, *109*, D11302, doi:10.1029/2003JD004501.
Yienger, J. J., M. Galanter, T. A. Holloway, M. J. Phadnis, S. K. Guttikunda, G. R. Carmichael, W. J. Moxim, and H. Levy II (2000), The episodic nature of air pollution transport from Asia to North America, *J. Geophys. Res.*, *105*(D22), 26,931–26,946.

H. Akimoto, Atmospheric Composition Research Program, Frontier Research Center for Global Change, JAMSTEC, 3173-25 Showa-machi Kanazawa-ku, Yokohama 236-0001, Japan. (akimoto@jamstec.go.jp)

K. Sudo, Graduate School of Environmental Studies, Nagoya University, Furo-cho Chikusa-ku, Nagoya 464-8601, Japan. (kengo@nagoya-u.jp)